Host University: Ghent University, Belgium
Faculty: Faculty of Engineering and Architecture
Department: Department of Structural Engineering and Building Materials
Academic Year 2020-2021

Numerical Modelling of Water Spray Impingement Cooling

Thushadh Wijesekere

Supervisor: Prof. dr. Tarek Beji

A Master's Thesis Submitted in the Erasmus Mundus Programme
INTERNATIONAL MASTER OF SCIENCE IN FIRE SAFETY ENGINEERING

Disclaimer

This thesis is submitted in partial fulfilment of the requirements for the degree of the *International Master of Science in Fire Safety Engineering (IMFSE)*. This thesis has never been submitted for any degree or examination to any other University/programme. The author declares that this thesis is an original work except where stated. This declaration constitutes an assertion that full and accurate references and citations have been included for all material, directly included and indirectly contributing to the thesis. The author gives permission to make this master thesis available for consultation and to copy parts of this master thesis for personal use. In the case of any other use, the limitations of the copyright have to be respected, in particular with regard to the obligation to state expressly the source when quoting results from this master thesis. The thesis supervisor must be informed when data or results are used.

Read and approved

Thushadh Wijesekere

Abstract

Out of the many computational fluid dynamics (CFD) packages available, Fire Dynamics Simulator (FDS) has been the most popular CFD package for fire scenarios. However, the predictions of FDS or any CFD package depends on the implemented models within the package for different scenarios. Some of these models have been validated using real life experimental work while some have not. The aim of the work presented is to asses (validate) the model used for heat transfer between water droplets and solid surfaces using a set of experimental work performed using a superheated copper (Cu) plate. Calculation of the convective heat transfer coefficient between the solid and the liquid phases was analysed for three different test cases.

The simulations were performed in a step-wise approach starting with simulations involving only the solid phase (Cu disc heated to 600 °C) and the water mist system individually before moving on to the simulations of the interaction of the water mist system and the Cu disc. Simulations were run using mono-disperse sprays due to the lack of information on the droplet size distributions.

The results show that FDS is indeed capable of producing relatively accurate results agreeing with the experimental work using mono-disperse sprays. This can be considered as the first step moving forward towards poly-disperse simulations where the droplet size distributions and the effects of the interaction of the plume and the water droplets can also be analysed.

Extended Abstract

The aim of the presented work was to carry out an assessment for a numerical model implemented in the much popular computational fluid dynamics (CFD) package, Fire Dynamics Simulator (FDS). The assessment focused on the water spray impingement cooling which is often referred to as 'surface wetting'. Convective heat transfer between a heated surface and water droplets deposited on the surface is a complex phenomenon in nature. Droplets dynamics on the surface provides more complexity due to movement, boiling and evaporation of the liquid. The same mechanisms in water spray impingement cooling results in much larger heat fluxes and heat transfer coefficients making it one of the most effective cooling mechanisms not just in fire safety but in many other industries as well.

Surface wetting in fire suppression is effectively used to cool down surfaces which are already in flaming combustion or surfaces that have not ignited but approaching the ignition temperature. The thesis presents an assessment of the heat transfer model used FDS version 6.7.5 for water cooling of a solid surface. The numerical simulations were inspired from a set of experimental work carried out using a copper (Cu) disc heated to 600 °C and a water mist system fixed 254 mm above the plate. After the activation of the water mist, the plate and the surroundings were allowed reach a steady state during which the plate temperature profiles, velocity and size distributions of the water sprays were measured using thermocouples and a phase Doppler particle analyser (PDPA).

The experiments include five different settings for the water mist system with three different water mass flow rates of 0.160 g/s, 0.385 g/s and 0.600 g/s and two extra different size distributions for 0.385 g/s set-up. The interaction of water droplets with the buoyant plume rising from the heated surface was highlighted in the experimental work by the size distributions and the velocity profiles during the steady conditions. It was therefore, decided to approach the simulations in a methodical manner starting with simulations with just the solid and water phases individually prior to considering the complete set-up.

The convective heat transfer model used for air convection in FDS was assessed using a separate set of experiments where FDS showed its capability of predicting accurate thermal field above a heated surface. Then, the 'lazy' buoyant plume generated by the Cu disc was analysed with respect to axial plume temperature, axial vertical velocity component of the gas phase and the radial temperature distribution just above the Cu disc. A grid sensitivity analysis was carried out for these parameters using cell sizes 10 mm, 5 mm and 2.5 mm. The results showed that the predictions were sensitive in the immediate vicinity of the Cu plate. However, above a certain height the predictions converged. All the simulations where only the Cu plate was considered were run using two different heat transfer models in FDS 6.7.5. Both the default model which is more dynamic and

a user specified constant heat transfer coefficient of $11.27 \, \mathrm{W}/(\mathrm{m}^2 \cdot \mathrm{K})$ were used in these simulations. Both models showed a non monotonic temperature profile above the Cu disc which led to a sensitivity analysis on the domain size used for the simulations. The size of the domain showed negligible effects on the results for the above mentioned flow and thermal field.

Due to the lack of data available on the water mist set-up used in the experiments, the modelling of the water spray was simplified by considering only mono-disperse sprays. Out of the five test cases, four of the test cases were simulated with a satisfactory output in terms of the temperature profile of the disc during steady state. However, the importance of poly-disperse spray simulations was identified since results were achieved adjusting the spray properties without attention to the sprays in the experiments. All of the water sprays were characterised by the upper limit of the experimental size distribution.

The work presented can be considered as the initial step towards a complete validation of the model for water spray impingement in FDS. Capturing well the properties of the water mist system in its original state for all the test cases is of great importance for a effective study. The author hopes the work done can be used as a reference for future work and eventually completing the model validation study.

Contents

List of Figures

List of Tables

Nomenclature

Acronyms

Al	Aluminium
CHTM	Convective Heat Transfer Model
Cu	Copper
CVF	Cumulative Volume Fraction
FDS	Fire Dynamics Simulator
HRR	Heat Release Rate
NFPA	National Fire Protection Association
PDPA	Phase Doppler Particle Analyser
ROT	Run-out Table
SS316	316 Stainless Steel

Dimensionless Numbers

Gr	Grashof number
Nu	Nusselt number
Pr	Prandtl number
Ra	Reyleigh number
Re	Reynolds number

Latin Characters

b	Plume radius	[m]
C	Constant for for geometry	-
F	Buoyancy flux	[m^4/s^3]
g	Gravitational acceleration	[m/s^2]
HV	`HORIZONTAL_VELOCITY`	[m/s]
h	Convective heat transfer coefficient	[W/(m$^2 \cdot$ K)]

k	Thermal conductivity	$[\mathrm{W/(m \cdot K)}]$
L	Characteristic length	$[m]$
M	Momentum flux	$[\mathrm{m^4/s^2}]$
Q	Mass flux	$[\mathrm{kg/s}]$
$\dot{q}$	Rate of heat transfer	$[\mathrm{W}]$
r	Radial distance	$[\mathrm{m}]$
T	Thermodynamic temperature	$[\mathrm{K}]$
u	Particle velocity	$[\mathrm{m/s}]$
$\mathbf{u}$	Velocity vector	$[\mathrm{m/s}]$
z	Height	$[\mathrm{m}]$

Greek Symbols

α	Entrainment coefficient (in plume parameter)	-
	Thermal diffusivity (in Prandtl number)	$[\mathrm{m^2/s}]$
β	Coefficient of thermal expansion	$[\mathrm{1/K}]$
Γ	Plume parameter	-
γ	`GAMMA_D`	$[\text{-}]$
ε	Surface emissivity	-
θ	Spray half angle	[degrees]
μ	`SPRAY_PATTERN_MU`	[degrees]
ν	Kinematic viscosity	$[\mathrm{m^2/s}]$
ρ	Density	$[\mathrm{kg/m^3}]$
σ	Stefan-Boltzmann constant	$[\mathrm{W/m^4 \cdot K}]$

Superscripts

$''$	Per unit area	

Subscripts

0	At the source	
∞	Ambient conditions	
$cond$	Conductive component term	
$conv$	Convective term	

ext	EXTERNAL_FLUX term
g	Gas phase
o	At the outer boundary
w	Vertical component
w	At the solid surface (phase)

Other Symbols

δn	Cell size in Fire Dynamics Simulator	[m]

Chapter 1

Introduction

In this chapter, based on similar work performed by researchers, an introduction to water spray impingement cooling and convective thermal plumes is provided alongside the motivation for the presented work and an outline of the thesis.

1.1 Background

Liquid water plays an integral role in fire suppression systems owing to its high latent heat of vaporization and high specific heat capacity in both liquid and vapour phases. In addition to its favourable thermal properties, it is also, non toxic and abundant almost everywhere in the world making it a very cost effective solution. Experiments related to the extinguishment of wood fires using water were done by Novozhilov et al. [1] which highlighted the importance of the 'surface wetting'. In this study, the authors also emphasize on the fact that droplet dynamics on the surface are vital to develop computational models for this specific scenario especially for low flow rates.

Spray impingement cooling is considered even in non-fire related applications as well due to its effectiveness in thermal management of solid surfaces usually associated with steel annealing and run-out table (ROT) cooling [2] in the steel industry. Steel stripes of temperatures around 1000 °C are cooled down with very high rates in these ROT applications [3][4]. These high rates of heat transfer associated with spray impingement cooling in general are due to the corresponding superior heat transfer coefficients in comparison to other cooling methods such as single phase natural and forced convection using air, fluorinerts and even water itself in the single phase region. This minimizes the amount of coolant consumed considerably relative to other impingement cooling techniques such as liquid jet cooling [5]. Figure 1.1 is a graphical depiction of magnitudes of heat transfer coefficients associated with these processes. Heat removal rates as high as $1 \, \text{kW/m}^2$ have been achieved previously using water as the coolant on surfaces with low superheat [6].

The importance of the interaction of heated surfaces and water droplets has been identified decades ago and several experimental studies have been carried out up to now [7][8][9]. Spray cooling starts with the liquid being forced through a small orifice which results in atomization of the liquid to fine droplets. These small droplets then come into contact with the heated surface and spreads radially where, high amounts of heat will be absorbed by the liquid phase. Eventually, the droplets vaporize after absorbing latent heat from the surface. The radial spread of liquid ensures uniform cooling of the surface [10].
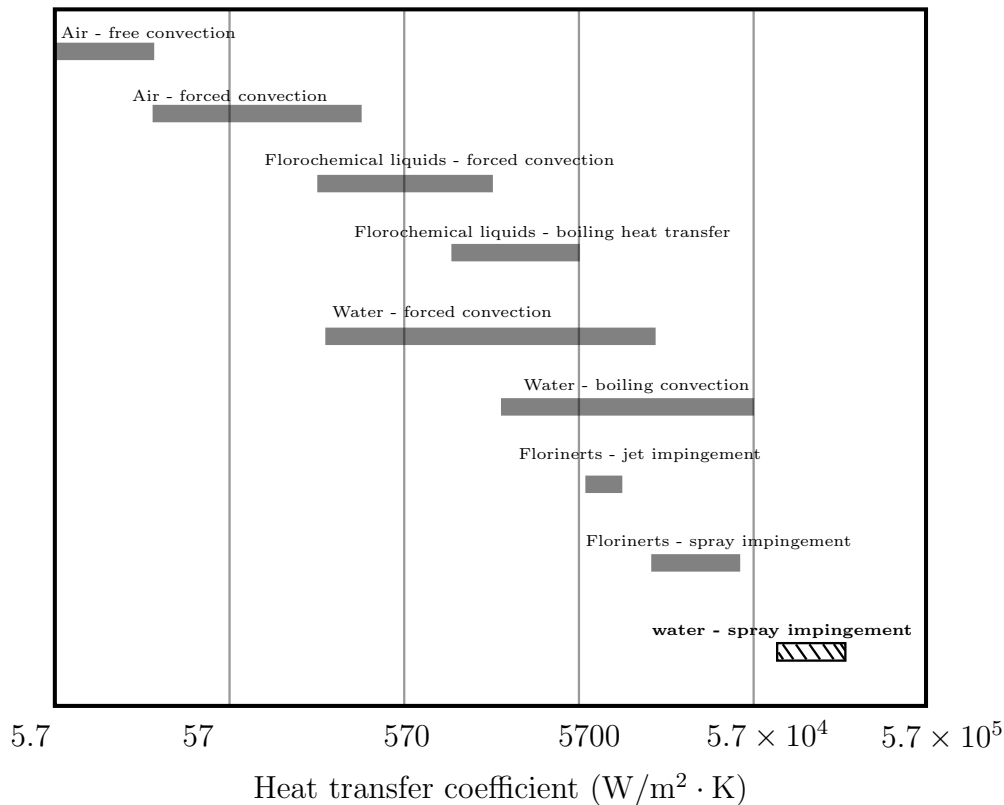
Figure 1.1: Heat transfer coefficients associated with different cooling techniques. Adapted from Nayak, Mishra, and Parashar (2016) [11].

The presence of heated surfaces in fire scenarios induces complex thermal and flow fields which are buoyancy driven. The effectiveness of the cooling depends on the interaction of the water droplets with the above-mentioned thermal and flow fields as the droplets might fully evaporate before reaching the surface or hit the surface with a high velocity and rebound upon impact. That is why the 'canonical' configuration studied in this work [12] consists of water droplets interacting with a so-called 'lazy' plume rising above a heated surface.

The interactions with the smoke layer and the heated (flaming) surface itself affect the fire in many ways as follows [13]:

- Evaporation of droplets before reaching the surfaces due to heat absorption from the hot gases.

- Inhibition of pyrolysis on the fuel surface after successful penetration of the fire plume.

- Surface cooling of walls, ceilings and the floor of the fire compartment.

- 'Pre-wetting' adjacent fuel packages limiting the potential spread of fire.

In addition to these mechanisms which aid the fire suppression, a portion of water droplets does not reach the smoke layer or fire, instead they are blown away.

In the following, a discussion on lazy plumes will be provided before addressing the topic of water sprays.

1.1.1   Lazy Plumes

The phenomena of convective plumes was first studied in 1941 by Schmidt [14] and was followed by a number of researchers in the area of meteorology [15][16][17] in the 1950's. Convective plumes, although usually produced by a source of heat, the phenomena is governed by the buoyancy aspects within the fluid [15]. Therefore, it is important to consider the properties of the fluid phase rather than considering only the heat source and its characteristics. Rouse, Yih, and Humphreys [15] initially performed an analytical and experimental study on the free convection from a point and line source, concluding that the plume characteristics can be analysed neglecting how the buoyancy effects are induced and also provided explicit correlations in the form of probability functions for axial velocity component and mass density gradients. These correlations showed the interdependency of the velocity and the density gradients which was also highlighted in the work done by Batchelor [17] two years later where he derived expressions for axial velocity, buoyancy acceleration and plume radius using dimensional analysis as functions of Prandtl number (Pr), radial and axial locations and weight *deficiency*. Interestingly, prior to this, these unknown functions were determined by Yih [18] for the special cases Pr = 1 and Pr = 2.

The most influential plume model in literature up to now was developed by Morton, Taylor Ingram, and Turner [16] in 1956 with several assumptions where power law relations were derived for reduced gravity and vertical velocity. These plume conservation equations were then modified with a virtual origin assumption to represent area sources of heat [19]. The first attempt to characterise free convective plumes was made in 1973 [20] using a parameter which is referred to as the plume source parameter (Γ_0) in the literature [21] and is defined as:

$$\Gamma_0 = \frac{5Q_0^2 F_0}{4\alpha M_0^{\frac{5}{2}}} \tag{1.1}$$

Where, Q_0, F_0, M_0 and α are respectively the dimensional mass flux, buoyancy flux, momentum flux and the entrainment coefficient for radial velocity at the plume boundary. If $\Gamma_0 > 1$; buoyancy fluxes are dominant therefore, 'lazy' plumes, $\Gamma_0 < 1$ for momentum driven 'forced' plumes and $\Gamma_0 = 1$ for 'pure' plumes.

The so called 'lazy' plumes are mainly driven by buoyancy forces, therefore, are associated with low velocities in the 'near source' region before accelerating with increasing plume height. This initial acceleration in the 'near source' region is mainly buoyancy driven due to the density gradients associated with heated air and not momentum driven for lazy plumes [22][23]. When this initial acceleration is coupled with low entrainment, the plume narrows itself to a 'waist' [20]. This peak velocity has been proven to occur where, $b\sqrt{\rho_\infty - \rho}$ is at its minimum by Fanneløp and Webber [24]. Here, b is the plume characteristic radius, ρ_∞ is the ambient air density and ρ is the plume density. They referred to this point as a 'neck' and mentioned that this 'neck' does not necessarily mean the minimum radius point of the plume and also could occur not in the physical region above the heat source.

A pure empirical correlation which agrees with this behaviour of axial velocity was proposed by Wang et al. [25] from experiments using particle image velocimetry. They val-

idated the correlation for different heat intensities and different sizes and shapes of heat sources. As per their experiments, when the temperature of the plate was low (around 50 °C), the maximum axial velocity was recorded at a height equal to the characteristic length of the heat source. However, this behaviour was not maintained at higher plate temperatures.

The region in the rising plume where, high gradients of vertical velocities and temperatures are recorded will be referred to as the 'near field' region and the region above it will be referred to as the 'far field' region throughout the thesis. A simple illustration of these regions alongside the coordinate system is shown in Fig. 1.2. When, the plume exits the near field region, the plume radius widens which causes the plume velocities to decelerate, while more air is entrained from the boundary bringing the plume temperature down due to mixing.
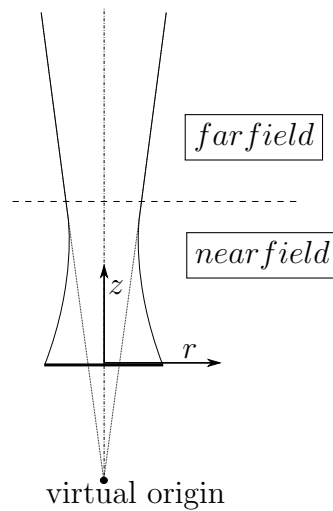
Figure 1.2: Regions within the rising plume.

Carlotti and Hunt [26] developed a plume model for lazy turbulent plumes in which the near field was successfully captured but with the assumption of a top hat profile. They also showed that the model predictions converge into the classical plume theory at the far field region.

Landers, Disimile, and Toy [27] also analysed the flow structures of plumes rising from flat circular stainless steel plates at varying temperature using schlieren imaging. They observed a flow being convected radially into the center of the plate before rising above the plate. They referred to the region with this initial radial convection as the boundary region, the region just above, as the near region which represents a transitional plume where the mixing of entrained air intensifies before turning into a fully developed turbulent plume in the far region. They made further analysis regarding the effect of plate temperature on the development of these three regions. When the plate temperature was increased, so did the rate of the development of the boundary layer and the momentum in the near field region. This resulted in achieving fully developed turbulence at a lower height. When the plate temperature was increased from 150 °C to 550 °C, the the height of the near field was reduced by 50% from 39 mm to 20 mm.

In a similar study [25], but with both circular and square sources of heat, using heated cast aluminium (Al) plates, Wang et al. observed the converging and diverging behaviour of the plume near the heat source and in the far field regions. For circular plates, random flow patterns were observed while, the converging flow near the source was observed along the partition lines and the diverging flow, from the edges of the plates for square heat sources.

The plume parameter is used to characterise plumes depending on the amount of buoyancy and momentum present at any height. The earlier mentioned source parameter represents the value of this parameter just above the heat source. The plume parameter as a function of plume height, $\Gamma(z)$ is defined as [21]:

$$\Gamma(z) = \frac{5Q^2(z)F(z)}{4\alpha M^{\frac{5}{2}}(z)} \tag{1.2}$$

Where, $Q(z)$, $F(z)$ and $M(z)$ are respectively, the mass flux, buoyancy flux and the momentum flux at plume height z. In theory, due to the lack of momentum flux near the source and high buoyancy effects, $\Gamma(z) > 1$ for all lazy plumes and $\Gamma(z) \gg 1$ for highly lazy plumes. Then, as the plume gathers momentum, $\Gamma(z)$ should decrease with height to value closer to 1. This asymptotic behaviour of plumes tending towards $\Gamma(\infty) \longrightarrow 1$ was first described in [20].

In recent studies, many have focused on the capability of CFD simulations to capture the near source behaviour of lazy plumes [28] [29] [30]. Taub et al. [29] and Hargreaves, Scase, and Evans [30] found out that $\Gamma(z)$ decreased to a near zero value initially before increasing to a value higher than unity and finally approaching unity in the far field region in the simulated results for lazy plumes. The assumption of a constant entrainment coefficient being not valid in the near source region of lazy plumes was highlighted and linked to this contradicting behaviour by Taub et al. [29] and both groups [29] [30] went on to show that the power law relations developed by Morton, Taylor Ingram, and Turner [16] for plume properties are only valid in the far field regions where, $\Gamma(z) \simeq 1$.

However, the model suggested by Carlotti and Hunt [26] implemented a simple entrainment model but was able to accurately predict the near source region as well. They labelled this model as the first model to produce accurate results for very lazy plumes in the near field region.

The contradictory statements and results from these recent studies show that the near field predictions of lazy plumes are still an ongoing discussion in the scientific community when it comes to both theoretical modelling and numerical simulations. The first part of this thesis focuses only on the simulations of the lazy plumes emerging from a heated Cu surface in Fire Dynamics Simulator (FDS) version 6.7.5.

1.1.2   Water Sprays in Fire Safety

Scientific work in understanding the extinction mechanism using water mist sprays in fire dates back to mid-nineteenth century [31] [32]. Most of the work carried out in this era have been purely experimental but considered both liquid and solid fuel fires [32] [33] [34] [35]. All of these experimental work focused mainly on the time for extinguishment. However, after the introduction of Halon 1301 and 1211 as chemical fire suppressants

which were more effective, the use of water as a fire suppressant reduced until bans were imposed regarding the environmental effects of halon fire suppressants [36]. The research work increased as the use of water as a suppressant was reinstated. This growth in attention towards water as a fire fighting agent is well described and proved in many surveys and studies [37] [38].

In the earlier studies related with the mechanism of fire suppression of water [31] [33], cooling down the flame by absorbing heat and oxygen displacement in the near flame region was identified. However, after a few decades, with advanced technology and experimental set-ups, the limitation of flame spread due to the attenuation of thermal radiation by the water droplets was also identified as a potential effective mechanism [39]. In the same study [39], Mawhinney, Dlugogorski, and Kim emphasizes on the importance of understanding the three main extinguishing properties of water by the computer model developers while, introducing two more less predictable mechanisms which should be taken into account in an ideal model. These three main properties, according to the authors were, heat extraction, O_2 displacement in the flame region, radiation attenuation by the water droplets and the two less predictable mechanisms included dilution of the combustible mixture below its lower flammability limit due to the entrained air from the spray and the intensification of the flames and consequently the heat release rate (HRR) of the fire immediately after the water spray has been introduced. This sudden increase of the HRR has been experimentally observed and has been linked to the increased turbulence in the flame region causing more vaporization of the fuel [39].

For water spray impingement cooling, the dominant extinguishing mechanism is heat extraction. Heat extraction by water droplets have been categorised from three possible regions in the fire: from hot flames and vapours, fuel packages yet to be ignited and from the fuel itself [39]. The latter two categories are more prominent and is the objective of impingement cooling. Water sprays have been classified in three classes by the National Fire Protection Association (NFPA) [40] depending on the cumulative percent distribution of the water droplet spectrum of the spray. Class 3 was deemed suitable for spray impingement cooling applications in fires. Class 3 was allocated to sprays which contained 90% of the total volume in droplets having a diameter greater than 400 µm but less than 1000 µm. The need for larger droplets in this size range is required in order to overcome the drag forces and the hydrodynamic effects of the plume before reaching the fuel surface [36].

The technique of water spray impingement, referred to as 'fuel wetting' in many studies [37] [39] [41] is applicable in fires with solid combustibles and is very effective for fuels that form a layer of char during combustion [39]. Even though, fuel wetting has been a key component of fire suppression, the experimental work related to this field is very limited, perhaps due to the poor documentation of experimental work. Some work is available in which hot metal plates have been used to represent burning surfaces [7] and heated objects in fires [42].

Performing full-scale fire experiments related with fire can be expensive and should be considered with caution given the uncertainties associated with the scaling effect [43] [44]. In addition, due to practical difficulties of performing such tests, the amount of experimental data is also rather sparse. With the rapid developments in computational power, com-

putational fluid dynamics (CFD) has gained popularity in fire research over the years [45].

Validation and verification are the techniques of measuring the accuracy of the physics and the mathematics in any computational model. The author is unaware of Validation studies performed for fuel wetting in FDS at this point. FDS is one of the most popular CFD packages in the fire safety field and has been validated in many areas [46] but not for the case of fuel wetting.

The second part of the work presented here is specifically focused on the interaction between a heated surface and impinging water droplets on it. The objective of the thesis is to perform an assessment study of FDS in order to analyse how the heat transfer between a heated surface and water droplets using FDS version 6.7.5. The work presented lays the ground work for the validation of the models implemented in FDS.

1.2   Thesis Outline

The second chapter begins with a brief overview of the experimental set-up and a thorough analysis on the convective heat transfer model implemented in FDS is also included which is followed by an extra set of simulations performed to further assess the capability of the default convective heat transfer model in FDS 6.7.5.

In the third chapter, the experimental set-up is introduced with its key components and major findings from the experimental work [7]. The discussion on the major finding focuses on the steady state plate temperature, size distribution of the spray and the velocity history with varying water mass flow rates, different distances from the heated surface and velocity and size distributions.

In the fourth, fifth and sixth chapters, results obtained from simulations with and without water mist system activation are presented and analysed both qualitatively and quantitatively. A grid sensitivity study for the gas phase axial plume temperature, axial velocity and the predictions of FDS in the near source region is presented. The effects of changing the size of the computational domain is also analysed prior to introducing water droplets.

The final chapter presents the conclusions derived from the work carried out and elaborates on the future work aiming towards a complete validation study.

Chapter 2

Methodology

In this chapter, the approach to the work is described in a comprehensive manner. The main methodology consists of considering the experimental work of Fu, Sojka, and Sivathanu [7] and assessing the FDS capabilities (regarding water impingement cooling) by comparing the simulation results against the available experimental data.

However, prior to considering the water impingement scenario, a series of preliminary simulations have been carried out by considering separately the lazy plume and the water spray.

Finally, it is important to mention that a particular attention has been given to the analysis of the convective heat transfer near the surface in the absence of water droplets.

2.1 Overview

The main focus of the work carried out is on the experimental work by Fu, Sojka, and Sivathanu [7]. The experiment was mainly focused on capturing velocity and size distribution history of a poly-disperse water spray while approaching a superheated Cu plate. The goal of the experiment, according to the authors, was to provide experimental data for validation purposes of models associated with interaction of water droplets and burning surfaces. A water spray approaching such a superheated surface will come across a buoyancy driven 'lazy' plume which will alter the flow field of the water droplets. droplet trajectory can also be affected by resulting evaporation during the residence time inside the buoyant plume. Finally, upon impact, the droplets will thermally interact with the hot surface leading to flame extinguishment, limitation of flame spread and surface cooling.

The documentation of the experimental work included the final results and outcomes. However, number of details required specifically for a validation study were not provided. Due to this reason, the setting-up of the computational input in FDS could not be executed directly. Several, different simulations had to be run with assumed values for many parameters related with the water mist system.

A set of simulations were performed as described in the following chapters, to assess the performance of FDS 6.7.5 in capturing the rather complex interaction between the hot plate and the water droplets. The approaching water droplets will interact with the hot plume above the heated Cu plate before making contact with the plate itself. The

interaction with the rising plume affects the impact velocity, size distribution at the plate surface, velocity distribution and approaching temperatures of the droplets. Therefore, the importance of the gas phase properties between the water mist nozzle and the plate was identified which led to dividing the total simulation into two main sections as follows:

1. simulations without water injection (solid-gas phases simulations)

2. simulations with water injection (solid-liquid-gas phases simulations)

In the upcoming sections these two sets of simulations are introduced.

2.1.1 Solid-Gas Phases Simulations

The modelling of the flow field and the temperature field above a heat source is still evolving due to its high complexity. The author is not aware of any validation work related to this specific configuration in FDS. Therefore, the initial simulations only included a heated Cu plate and the surrounding gas phase. The axial plume temperature variations, velocity profiles in the axial direction and the radial temperature variations of the solid phase and the gas phase just above was analysed for these simulations. The convective heat transfer model used in FDS was put to test against an additional test case which involved a stainless steel plate of similar dimensions [27].

2.1.2 Solid-liquid-Gas Phase Simulations

After satisfactory results were obtained for the solid and gas phases, the water mist system was introduced into the simulation environment. These simulations were set up such that, it represents the experimental set-up. Initially, the water mist spray was modelled as a mono-disperse spray before moving on to poly-disperse sprays.

2.2 Convective Heat Transfer Models in FDS 6.7.5

The prediction of the velocity and thermal profile of the free convective lazy plume rising from the heated surface is heavily dependent on the convective heat transfer coefficient between the heated surface and the air layer just above. Not only is the convective heat transfer coefficient important in the prediction of the conditions above the plate, but this parameter is also vital when modelling the heated Cu plate in FDS to achieve the desired surface temperature.

As per the FDS user's guide [47], there are several possible methods in FDS to model a heated surface at a constant temperature; the most straightforward method being directly imposing the desired temperature by setting `TMP_FRONT` to a value on the `SURF` line. This method does not consider the material properties, the dimensions of the surface and the environment around but will maintain the temperature at the set value. It was, therefore decided that this method will not be suitable for the continuation of this work.

The next method is to specify `EXTERNAL_FLUX` on the SURF line to provide a heat source on the Cu plate which heats up the plate to the desired temperature. This method does take into account the material properties, dimensions and the interaction with the surrounding environment. However, the heat transfer calculations will be performed in

FDS based on the user input. Therefore, to make a rough estimation of the required input for EXTERNAL_FLUX, a simple heat transfer hand calculation was done. Figure 2.1 shows how the plate interacts with the external heat source and the environment at steady state.
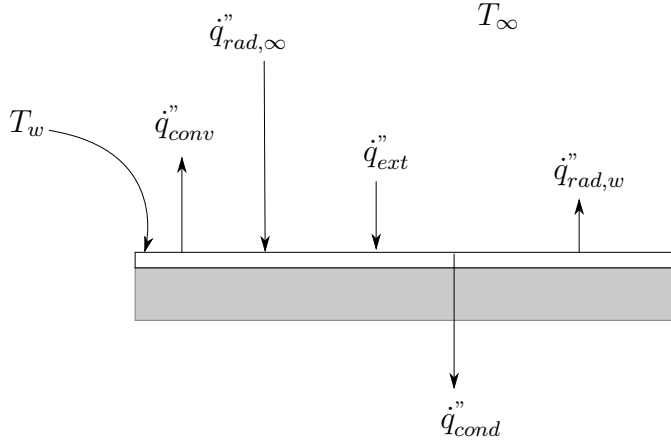
Figure 2.1: Schematic representation of the Cu plate, showing the heat transfer processes. T_w, temperature of the heated surface; T_∞, ambient temperature; $\dot{q}''_{conv}$, convective heat flux from the surface to the atmosphere; $\dot{q}''_{rad,\infty}$, radiative heat flux from the surroundings to the surface; $\dot{q}''_{ext}$, EXTERNAL_FLUX term; $\dot{q}''_{cond}$, conductive heat flux to the backing of the plate, $\dot{q}''_{rad,w}$, radiative heat flux from the plate to the surroundings.

The conductive heat losses to the backing was set to zero by setting BACKING='INSULATED' on the FDS input. The Cu plate was also assumed to be thermally thin. This was confirmed by the internal temperature profile of the Cu plate. The energy balance on the heated surface at steady conditions derives:

$$\dot{q}''_{ext} = \varepsilon\sigma\left(T_w^4 - T_\infty^4\right) + h\left(T_w - T_\infty\right) \tag{2.1}$$

where, ε is the emissivity of the heated Cu surface which was set to 0.78 [48], σ is the Stefan-Boltzmann constant which is equal to $5.67 \times 10^{-8}\,\mathrm{W/m^4 \cdot K}$, h is the convective heat transfer coefficient between the atmosphere and the heated surface which was calculated using $T_w = 873\,\mathrm{K}$ and $T_\infty = 293\,\mathrm{K}$. For this calculation, the Grashof number, Gr was used which is a dimensionless parameter representing the ratio between buoyancy forces in a fluid to the viscous forces and is defined as:

$$\mathrm{Gr} = \frac{g\beta\left(T_w - T_\infty\right)L^3}{\nu^2} \tag{2.2}$$

Where, g is the gravitational acceleration, $\beta = 1/T_\infty$, L is the characteristic length of the plate which is $0.2\,\mathrm{m}$ and the kinematic viscosity is given by ν. Another dimensionless parameter, the Prandtl number which is the ratio of the momentum diffusivity and the thermal diffusivity was also used in the calculation. The Prandtl number, Pr is simply defined as:

$$\mathrm{Pr} = \frac{\nu}{\alpha} \tag{2.3}$$

Where, α is the thermal diffusivity. The Nusselt number, Nu can then be calculated depending on the configuration of the solid phase using Gr and Pr. For natural convection from a horizontal flat plate, Nu is defined as [49]:

$$\text{Nu} = 0.14 \, (\text{Gr} \cdot \text{Pr})^{\frac{1}{3}} \tag{2.4}$$

The Nusselt number is also defined as the ratio of convective and conductive heat transfer through a fluid and this definition leads to:

$$\text{Nu} = \frac{h}{k/L} \tag{2.5}$$

Where, k is the conductive heat transfer coefficient of the fluid. Combining the two definitions for Nu (Eqns. 2.4 & 2.5) leads to a direct estimation for the convective heat transfer coefficient, $h = 11.27 \, \text{W}/\left(\text{m}^2 \cdot \text{K}\right)$. For this calculation, the properties of the gas phase were calculated using 1/3 rule for film temperature. The estimate for the EXTERNAL_-FLUX term was $31.9 \, \text{kW/m}^2$.

Several models are made available in FDS to model the heat transfer coefficient for natural convection. The default model in FDS uses a combination of both natural and forced convection which uses local Reynolds numbers at the surface using fluid velocities. The default model in FDS 6.7.5 calculates convective heat flux in units W/m^2 as:

$$\dot{q}_{conv}^{''} = h \, (T_g - T_w) \tag{2.6}$$

Where, T_g and T_w are the gas phase temperature and surface temperature of the solid phase respectively. The convective heat transfer coefficient, h is calculated in $\text{W/m}^2 \cdot \text{K}$ as:

$$h = \max \left\{ C \, |T_g - T_w|^{\frac{1}{3}}, \; \frac{k}{L}\text{Nu}, \; \frac{k}{\delta n/2} \right\} \tag{2.7}$$

Where, C is 1.52 for horizontal flat plates, k is the thermal conductivity of the fluid, L is the characteristic length of the plate which is 200mm for this case, $\delta n/2$ is the cell size and the Nusselt number, Nu is defined as:

$$\text{Nu} = C_1 + C_2 \text{Re}^n \text{Pr}^m \tag{2.8}$$

By default, the values for C_1, C_2, n, m are set to 0, 0.037, 0.8 and 0.33 respectively for planar surfaces. The Prandtl number, Pr is set to 0.7 by default while, the Reynolds number, Re is calculated in FDS.

The calculation of h in FDS was further investigated to understand the logic behind this calculation method in FDS using the provided references in [47]. The first element in the set is an empirical correlation suggested by Holman in [50]. However, the range of applicability suggested in [50] is for Rayleigh number, $\text{Ra} > 10^9$. Rayleigh number is the product $\text{Gr} \cdot \text{Pr}$. The second element of the set is linked to the calculation of Nu using the Reynolds number, Re which is used in forced convection. This definition of Nu is applicable under complete turbulent boundary layer conditions [51]. Substituting h in Eq. 2.6 by the final element in 2.7, the Fourier's law for heat conduction is obtained. This implies the heat transfer process is being treated as if the heat was conducted to the

center of the gas phase cell just above the solid surface.

In this default model, the maximum value for h calculated using Eq. 2.7 is used for heat transfer calculations in FDS. If natural convection is dominant, the second component will be neglected due to low velocities involved in that scenario and vice versa. However, if the cell size is fine enough, the calculation can shift to a conduction problem regardless of the the nature of convection in the simulation.

There is also the possibility for the user to specify a constant value for h throughout the simulation using `HEAT_TRANSFER_COEFFICIENT` on the `SURF` line with units of $W/(m^2 \cdot K)$. This is somewhat similar to imposing a constant surface temperature in FDS. However, this is useful when comparing the hand calculations with the simulated results.
`HEAT_TRANSFER_COEFFICIENT = 11.27` setting was used for the constant heat transfer coefficient simulations which corresponds to the value obtained in the hand calculations.

A special model specifically for heat convection from the curved surfaces of long horizontal cylinders is also made available which is not applicable for the case at hand.

Even though, in conventional calculations, the Rayleigh number, Ra is used to calculate the convective heat transfer coefficient, h for natural convection, a different model is used in FDS which uses both natural and forced convection in addition to pure heat conduction to determine h. The inability of FDS to resolve the boundary layer and the use of these simplified empirical correlations derived for very specific cases has been pointed out by Veloo and Quintiere [52] in 2013. This calls for a critical analysis of the calculation method used in FDS in order to analyse the overall accuracy of model with respect to the prediction of flow and thermal field over the heated plate.

2.3   Assessment of Predictions of Thermal and Flow Field above a Heat Source in FDS

Due to the simplifications used in the convective heat transfer model utilized in FDS and its limited applicability for natural convection, additional simulations were run related to experimental work done by Landers, Disimile, and Toy [27] considering the thermal field above a flat superheated 316 stainless steel (SS316) disc with a diameter of 200mm and a thickness of 1.27 cm. The predictions on FDS for this set up will provide a good benchmark for the prediction of the lazy plume rising from heat source.

Simulations were run using 2 different grid resolutions: 10 mm and 5 mm . The computational domain was set to 300 mm × 300 mm × 300 mm. The SS316 plate was placed centrally 5 cm above the bottom surface of the computational domain as sown in Fig. 4.1. To speed up the calculations to reach steady state, `TIME_SHRINK_FACTOR=10` was used in all the simulations. The total simulation time was set to 2500 s to provide at least 500 s of steady conditions. The computational domain is sketched in Fig. 2.2 with the dimensions and the orientation of SS316 plate.
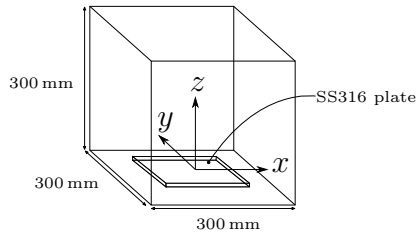
Figure 2.2: Schematic representation of the computational domain in FDS with the SS316 plate. (Not to scale.)

The SS316 plate was modelled as a square plate with a thickness of 5 mm and the length of 200 mm which is identical to the diameter of the cylindrical plate used in the experiments. The thermal properties of SS316 are given below in Table 2.1.

Table 2.1: Thermal properties of SS316

Thermal conductivity	17	$W/(m \cdot K)$
Specific heat capacity	0.49	$kJ/(kg \cdot K)$
Density	8070	kg/m^3

Note: All values obtained from AZoM [53].

The emissivity of SS316 was set to 0.57 [54]. The SS316 plate was heated to different temperatures.

The simulated results and the experimental data are shown below in Fig. 2.3 for different cell sizes (δn) in FDS.
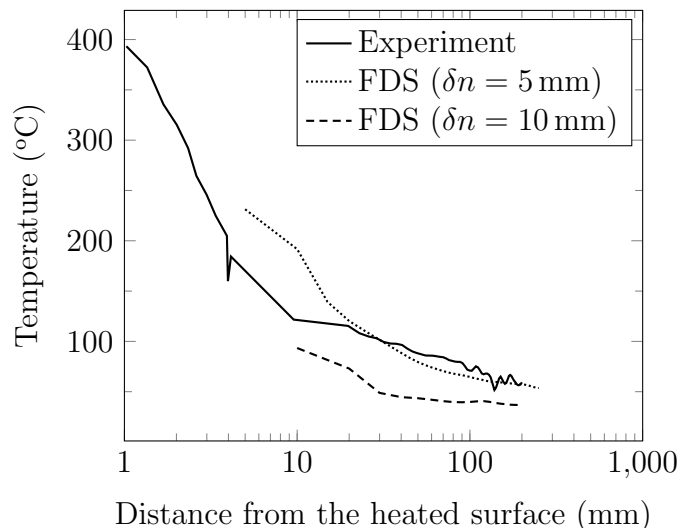
Figure 2.3: Temperature profile over the heated plate. Experimental data was extracted from Landers, Disimile, and Toy (2017) [27].

The 10 m grid resolution has under-predicted the temperatures of both near the heated plate and away from the heated plate. Major improvement is seen when the grid resolution

was in increased to 5 mm in both regions, however, still, the near source region is not well captured but over predicted with the 5 mm grid resolution.

Chapter 3

Experimental Set-Up

This chapter includes a detailed description of the experimental apparatus used by Fu, Sojka, and Sivathanu [7] and their major findings from the experiments.

3.1 Experimental Apparatus

The case at hand involves water droplets released form the water mist nozzle coming into contact with a heated Cu plate. The Cu plate is cylindrical in shape with a diameter of 200 mm and a thickness of 5 mm and is heated to a surface temperature of around 600.9 °C. The surface temperature distribution has an average of 600.9 °C and a standard deviation of 2.9 °C. The effervescent spray nozzle produces a solid spray cone and is located 254 mm above the heated surface along the axis of the cylindrical plate.

The complete experimental set-up consisted of a spiral wound resistance heater to heat up the Cu plat, a phase Doppler particle analyser (PDPA) for measuring water droplet size and velocity distributions and thermocouples for temperature measurements as shown in Fig. 3.1.
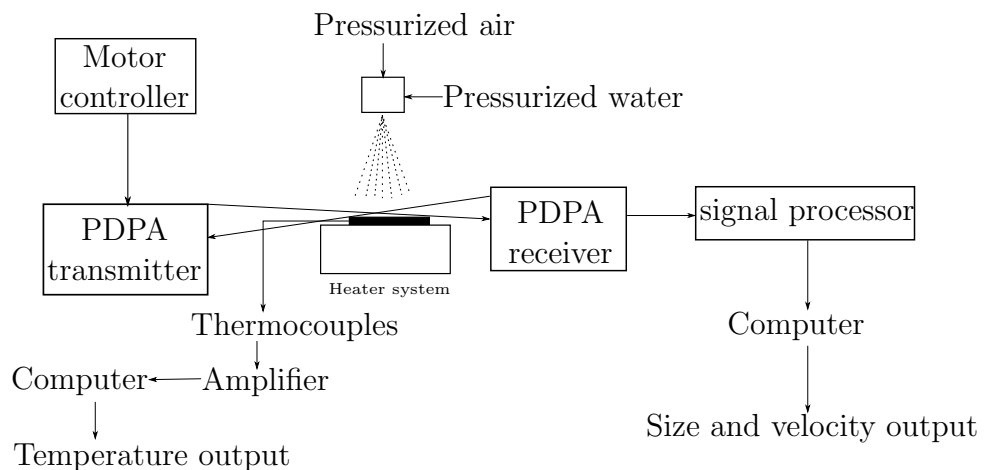
Figure 3.1: Schematic of the complete experimental set-up including the measuring devices. Adapted from: Fu, Sojka, and Sivathanu (1999) [7].

The steady state surface temperature of the heated surface has been measured at different

radial locations using five K-type thermocouples as shown in Fig. 3.2 on the surface while altering the water flow rates, droplet size distributions and droplet velocities. The droplet size distributions for different flow rates have been measured at 4 mm above the heated surface. In addition, the size distributions of the droplets have been measured at different heights for constant flow rate of 0.385 g/s. Finally, the velocity profiles of the original spray without the heated surface at 250 mm downstream the nozzle has been compared with the profiles in the presence of the heated plate at 250 mm and 190 mm downstream of the nozzle.
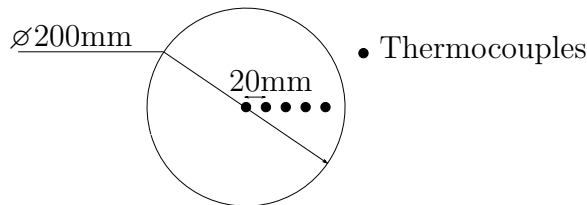
Figure 3.2: Schematic of the thermocouple set-up on the plate. Adapted from Fu, Sojka, and Sivathanu (1999) [7].

3.2 Major Findings

The main results from the experiments are presented in this section. All the results presented here are extracted from the documented experimental work published in "On the Interaction Between Evaporating Sprays and Heated Surfaces" by Fu, Sojka, and Sivathanu [7].

As explained in the section above, temperature readings on the heated surface was recorded at five locations. The main focus has been directed at the steady state temperature distribution on the plate surface, size distribution of the water spray 4 mm above the heated surface and the velocity distribution of the spray. Different test conditions were imposed by altering the water and air flow conditions.

3.2.1 Plate Temperature

The plate temperature was maintained around 600 °C prior to the introduction of water spray. The influence of the water flow rates and size and velocity distribution were analysed.

The water flow rates were changed in the spray while maintaining a consistent size and velocity distributions. Three different flow rates were used in experiment: 0.160 g/s, 0.385 g/s and 0.600 g/s. For the lowest flow rate, the very fine droplets were evaporated even before reaching the plate and uniform cooling of the plate was observed due to the lack of bouncing off from the plate and water deposition. Even though, there was uniform cooling, the plate temperature was not greatly reduced. Lower plate temperatures were recorded when the flow rates were increased. However, due to the water deposition near the center of the plate, uniform cooling was not achieved. The plate temperature was lower in the center and gradually increased in the radial direction. The temperature difference at the center and 80 mm away from the center is over 150 °C for both higher

flow rates. The results are shown in Fig. 3.3 (Right) with the size distributions using the Sauter Mean Diameter (SMD) on Fig. 3.3 (Left).
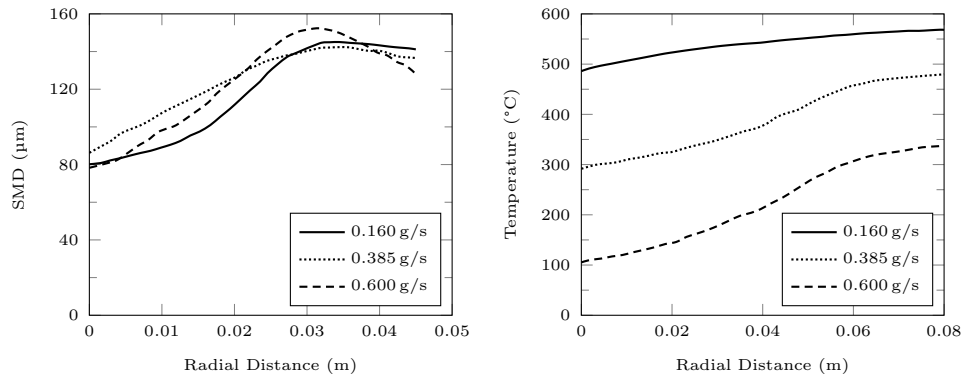
Figure 3.3: Original size distributions of the sprays and the steady state plate temperature. Left: Size distributions. Right: Plate temperature profiles in steady state. Experimental data was extracted from Fu, Sojka, and Sivathanu (1999) [7].

After the activation of the water mist system, during the steady conditions, the size distributions of each of the above sprays were measured 4 mm above the plate surface. The recorded results are shown in Fig. 3.4.
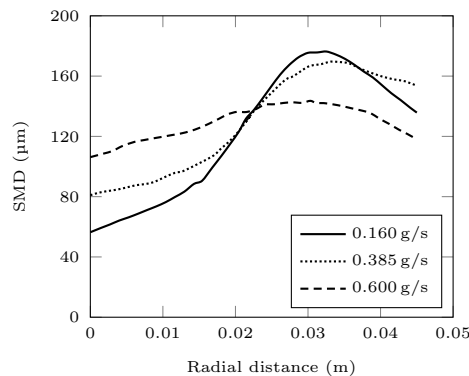
Figure 3.4: Size distributions of the water spray 4 mm above the plate. Experimental data was extracted from Fu, Sojka, and Sivathanu (1999) [7].

Three different size and velocity distributions [See Fig. 3.5 (Left)] were set by regulating the air pressure and flow rate with a constant water flow rate of 0.385 g/s. The finer droplets approached the plate at higher velocities which resulted in bouncing off the surface once the droplets hits the surface. On the other hand, the larger droplets were easily deposited on the surface increasing the cooling effect of the spray. This resulted in more efficient heat transfer to the water droplets hence, a larger temperature drop as shown in Fig. 3.5 (Right).
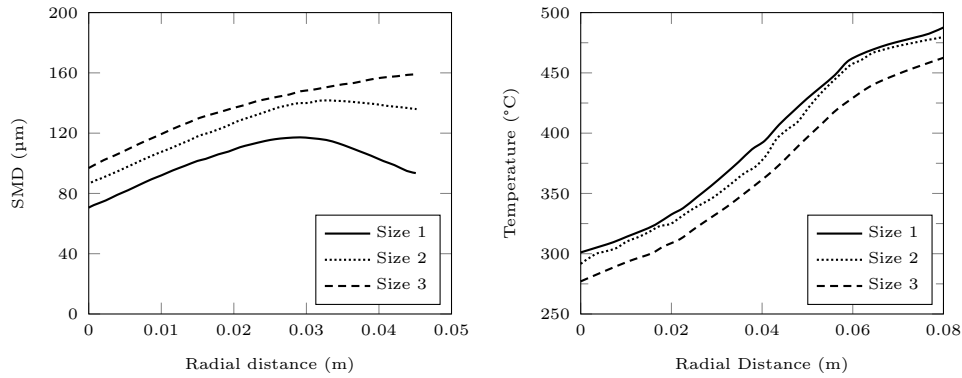
Figure 3.5: Size distributions of the water spray and the steady state plate temperatures at 0.385 g/s in the experiment. Left: Size distributions. Right: Plate temperature profiles in steady state. Experimental data was extracted from Fu, Sojka, and Sivathanu (1999) [7].

For the above sprays, the size distribution was measured 4 mm and 64 mm above the plate. The results are shown below in Fig. 3.6.
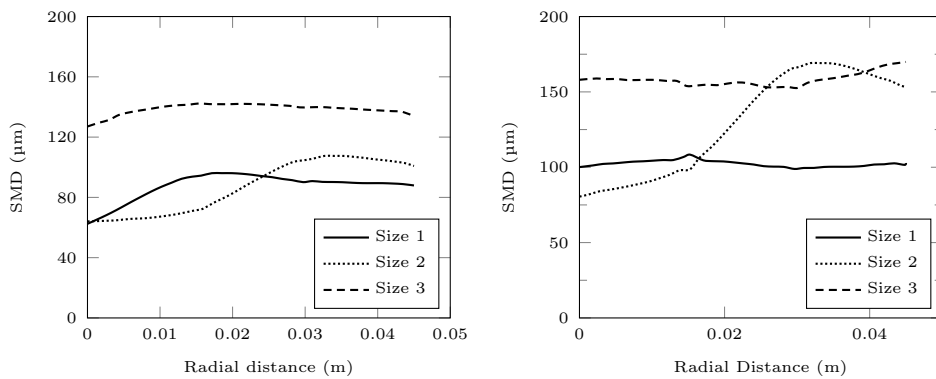
Figure 3.6: Size distributions of the spray at different heights above the plate. Left: 4 mm above. Right: 64 mm above. Experimental data was extracted from Fu, Sojka, and Sivathanu (1999) [7].

It was observed that the mean sizes of the droplets are higher closer to the heated surface due to the evaporation of smaller droplets. Additionally, the PDPA recorded also showed a rapid decline in the smaller droplets and a more gradual decline of the larger droplets. The rapid decline is due to evaporation of the full droplet and the gradual decline is due to the partial evaporation of larger drops.

Figure 3.7 shows the velocity distributions of the original spray and the distributions at steady state at different 4 mm and 64 mm was also presented for the 'size 2' case in the Fig. 3.5.
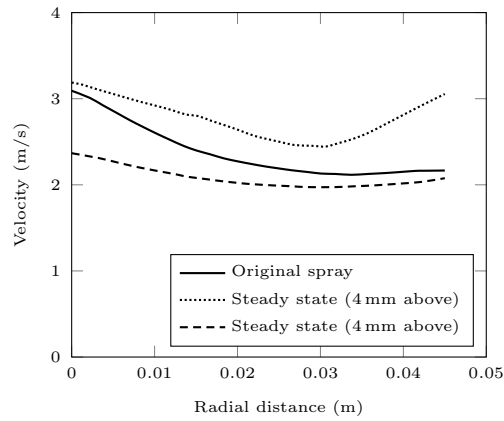
Figure 3.7: Velocity distributions of the water spray above the plate. Experimental data was extracted from Fu, Sojka, and Sivathanu (1999) [7].

Compared to the original spray, the velocities initially dropped at 64 mm above the plate before increasing 4 mm above the plate. The sudden increase of the velocities is due to the more weight put on the mean values by the larger droplets near the plate and the evaporation of the finer droplets simultaneously.

Chapter 4

Flow and Temperature Field Predictions Above the Hot Plate

The chapter begins with a presentation of the computational set-up of the solid-gas simulations followed by introduction to the settings and simulation ID keys to each test case which are used in the results and discussion section. The results analysis starts off with a qualitative analysis on the plume temperature and axial velocity which is followed by quantitative analyses in the forms of a grid sensitivity study for gas phase properties and a comparison of the used convective heat transfer models in FDS.

4.1   Computational Set-Up

The capability of predicting the interaction between the water droplets and the heated plate depends on the predicted flow and thermal field over the heated Cu disc because of the strong influence on the droplet sizes and the droplet temperatures at point of impingement. Therefore, it is essential to analuse the predictions in FDS with just the heat source before considering the injection of water droplets.

Simulations were run using 3 different grid resolutions: $10\,\mathrm{mm}$, $5\,\mathrm{mm}$ and $2.5\,\mathrm{mm}$. The computational domain was set to $300\,\mathrm{mm} \times 300\,\mathrm{mm} \times 300\,\mathrm{mm}$. The Cu plate was placed centrally $5\,\mathrm{cm}$ above the bottom surface of the computational domain as sown in Fig. 4.1. The steady state parameters of the heated plate is the focus in this work, therefore, to speed up the calculations to reach steady state, `TIME_SHRINK_FACTOR=10` was used in all the simulations. The total simulation time was set to $2500\,\mathrm{s}$ to provide at least $500\,\mathrm{s}$ of steady conditions.
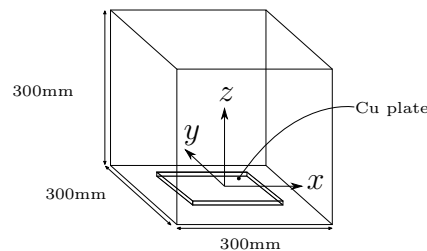
Figure 4.1: Schematic representation of the computational domain in FDS with the Cu plate. (Not to scale.)

The Cu plate was modelled as a square plate with a thickness of 5 mm and the length of 200 mm which is identical to the diameter of the cylindrical plate used in the experiments. The thermal properties of the Cu plate are tabulated below in Table 4.1.

Table 4.1: Thermal properties of Cu.

Thermal conductivity	401	$W/m \cdot K$
Specific heat capacity	0.385	$kJ/kg \cdot K$
Density	8960	kg/m^3

Note: All values obtained from [55].

The emissivity of the Cu surface was set to 0.78 to represent a Cu surface which is heated and covered with a thick oxide layer [48].

Measurements for temperature and vertical velocity were recorded in FDS and the results are discussed in the following section. The simulations IDs provided in Table 4.2 are used in this discussion.

Table 4.2: Settings of simulations without water.

Simulation ID	Convective heat transfer model (CHTM)	Cell size $[\delta n](mm)$
DM-10	Default	10
DM-5	Default	5
DM-2.5	Default	2.5
CH-10	$h = 11.27\,W/\left(m^2 \cdot K\right)$	10
CH-5	$h = 11.27\,W/\left(m^2 \cdot K\right)$	5
CH-2.5	$h = 11.27\,W/\left(m^2 \cdot K\right)$	2.5

4.2   Results and Discussion

The results from FDS simulations for all test cases without injection of water are presented and discussed in this section both qualitatively and quantitatively.

4.2.1   Heated Surface

The basis for all the generated results for gas phase is dependent on the surface temperature of the heated Cu surface in the steady state. The steady state plate temperature profile in the radial direction for each case can be found on Table 4.3 where, r is the radial distance from the center of the Cu plate.

Table 4.3: Steady state radial plate temperature profiles. Experimental data extracted from Fu, Sojka, and Sivathanu (1999) [7].

r (m)	0	0.2	0.4	0.6	0.8
	Surface temperature (°C)				
Experiment	598.7	600.2	602.4	605.9	597.5
DM-2.5	604.8	604.5	603.8	602.6	599.0
DM-5	602.6	602.5	602.0	601.3	598.0
DM-10	602.8	602.6	602.2	601.7	598.9
CH-2.5	600.7	600.6	600.3	599.8	598.2
CH-5	603.0	603.0	602.7	602.2	600.2
CH-10	600.9	600.8	600.4	600.0	598.4

The steady state plate temperature profile in a FDS simulations are in good agreement with the experimental data. This provides a great basis for the comparison of gas phase and liquid phase properties between the experiment and FDS.

4.2.2 Qualitative Analysis

The plume temperature profile and the vertical velocity along the center line of the plume will be assessed under this section. The time averaged velocity and temperature profiles above the heated Cu plate is shown below in
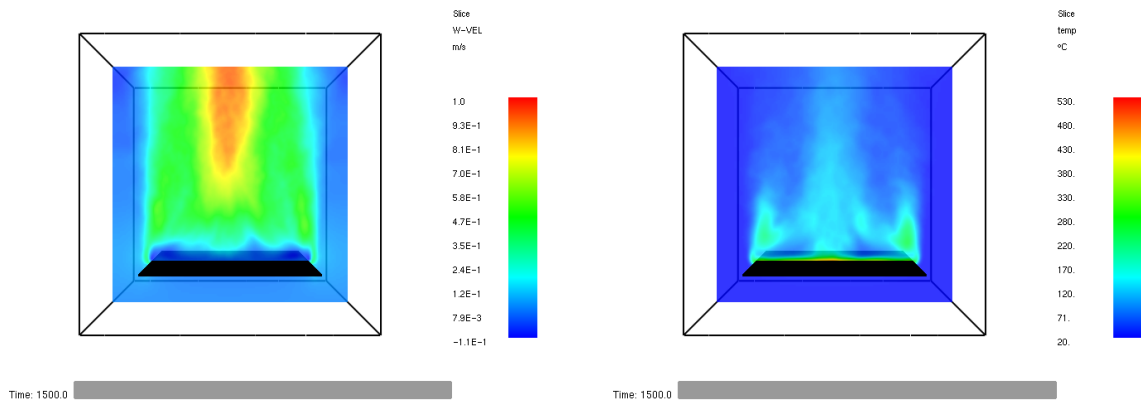
Figure 4.2: Time averaged steady state profiles. Left: Vertical velocity. Right: Plume temperature.

The vertical velocity along the axis starts with low magnitudes which represents a lazy plume with low momentum flux and the flow is accelerated as the plume height increases until the top boundary of the computational domain. The temperature profile on the other hand, starts at higher values and decreases rapidly with the plume height due to entrainment of fresh air as the plume moves upwards.

From a qualitative point of view, FDS has successfully captured the near source velocity field. Similarly, from purely qualitative point of view, the temperature profile of the

buoyant plume rising from the heated plate is also captured showing a reduction of temperature with height. However, it should be noted that the 'necking' of the lazy plume at the interface of the near field and the far field is not visible in the slice file data of the FDS output. This might be due to the the domain being not larger enough in the z direction to include this point in the plume. In order to get a clearer picture, the results are analysed quantitatively in the following section.

4.2.3 Grid Sensitivity Analysis for the Gas Phase

Axial Temperature

The grid sensitivity of the plume temperature along the axis of the cylindrical disc is discussed in this section. The plume temperature along the center line will determine the approaching temperature of the water droplets which impact on the heated surface. The plume temperature, therefore, is a parameter which has an impact on the cooling effect of the water spray. The simulated results for plume temperature is for both CHTMs are illustrated in Fig. 4.3.
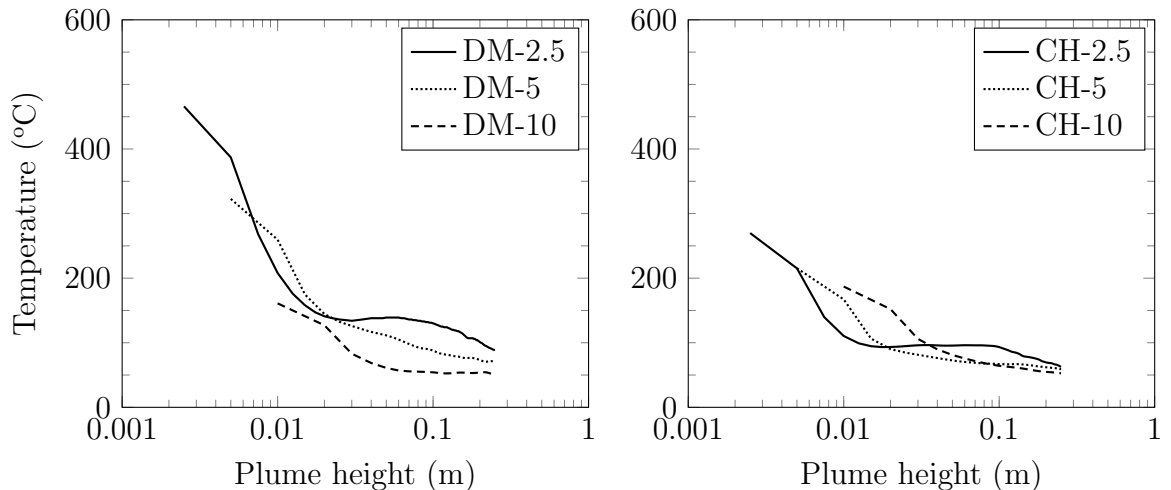
Figure 4.3: Axial plume temperature profiles at steady state. Left: default CHTM. Right: $h = 11.27 \, \mathrm{W/(m^2 \cdot K)}$.

For both CHTMs, the near field predictions barely above the heated surface shows a larger sensitivity compared to the region above 10 cm. However, in the default model, the coarse grid ($\delta n = 10 \, \mathrm{cm}$) shows a larger deviation from the rest of the grid sizes. In the region above 10 cm, for the default model only the two finer grids have shown convergence, while all three grid sizes have produced results without as large a deviation for the specified constant convective heat transfer coefficient. It is clear that when all the cell sizes are assigned the same heat transfer coefficient, it is only the very near field prediction that is more sensitive to the grid size. The default CHTM used in FDS 6.7.5 is also dependent on the grid size as mentioned in Eq. 2.7, therefore, the larger sensitivity of the default model in the far field can be due to the change in the calculation of h.

The deviation of the very near field predictions have shown a large variations when the grid was changed for both CHTMs, but, the deviation is very minimal for the two finer meshes in the constant h case. The highest temperature in that region is recorded around

380 °C for grid sizes 5 mm and 2.5 mm.

During the steady conditions, it can be seen that the temperature profiles have not shown a monotonic decline in both models. It is difficult to say what this behaviour can be associated with right now but, a sensitivity analysis on the domain size can show possible causes that affect the side entrainment of ambient air into the lazy plume. Furthermore, increasing the simulations times and averaging the temperatures over an even longer period of time might produced improved results.

Axial Velocity

The results of the grid sensitivity study of vertical velocity component ($\mathbf{u}_{\mathrm{w}}$) of the gas phase is presented in this section. Similar to the temperature measurements, $\mathbf{u}_{\mathrm{w}}$ was also measured along the vertical axis of the Cu plate. Figure 4.4 depicts the results of the simulations for both CHTMs.
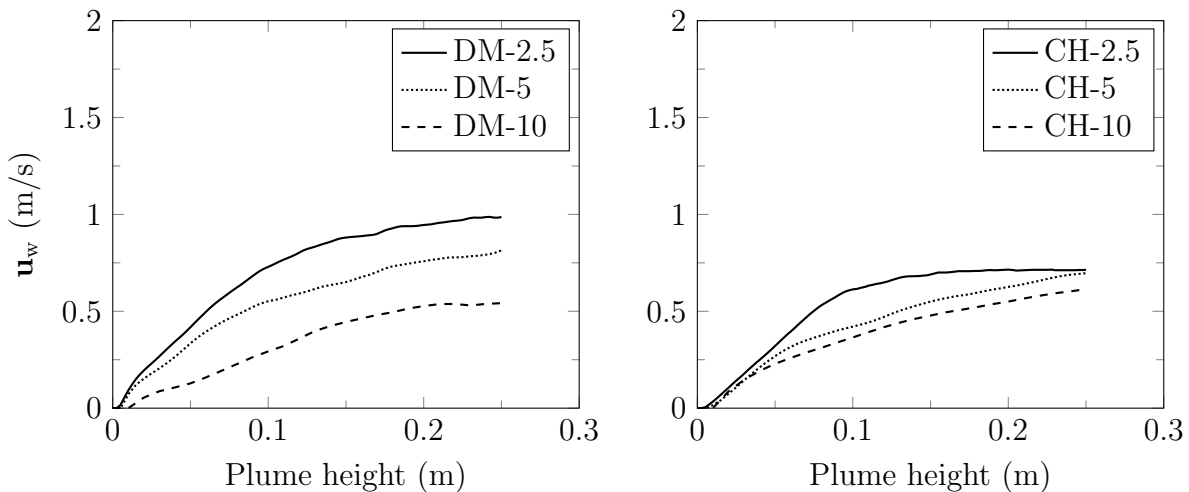
Figure 4.4: $\mathbf{u}_{\mathrm{w}}$ profiles at steady state. Left: default CHTM. Right: $h = 11.27 \, \mathrm{W/m^2 \cdot K}$.

As expected for the lazy plumes, all simulations show negligible initial velocity at the heated surface. FDS has been able to capture the pure buoyancy driven flow field at the surface. However, as the plume height is increased the predictions have deviated depending on the grid size. The $\mathbf{u}_{\mathrm{w}}$ predictions have been less sensitive to the grid resolution for the constant h simulations as opposed to the default CHTM simulations where the two finer meshes show a large deviation from the coarse grid. This behaviour was also observed in the temperature profiles and the two behaviours are definitely linked. Lower temperature predictions in the coarse mesh for default CHTM has similar lower $\mathbf{u}_{\mathrm{w}}$ predictions due to less buoyancy as expected. Similar to the temperature profiles, the sensitivity can also be linked to the CHTM used in as default in FDS. The codependency of the temperature field and the flow field is well captured in the simulations, but, the dependency of these predictions on the CHTM used for the calculations has to be analysed further.

Radial Temperature Profile Near the Heat Source

The gas phase temperature just above the heated surface is analysed under this section. The initial step of heat convection happens at this level, which the calculation performed

for the regions above are based upon. The radial temperature distribution for the default CHTM over the Cu plate at $z = 0$ is presented in Fig. 4.5.
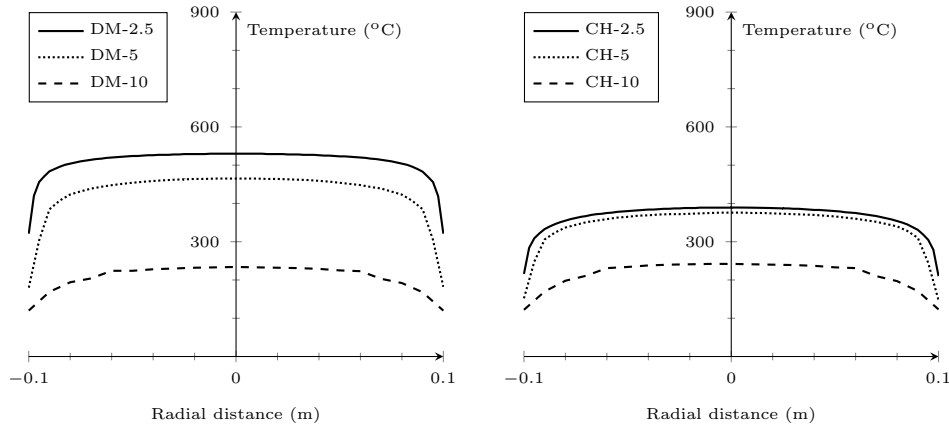
Figure 4.5: Radial temperature profile of the gas phase at $z = 0$. Left: default CHTM. Right: $h = 11.27 \, \text{W}/\left(\text{m}^2 \cdot \text{K} \right)$.

The radial temperature distribution of the gas phase is almost uniform across the length of the plate for all cell sizes in both CHTMs even though the recorded temperature shows a deviation when the grid resolution is changed. For, the default CHTM, 2.5 mm grid shows readings just above 500 °C across the length but, lower values have been recorded for the other two grids (5 mm and 10 mm). The temperatures are around 450 °C for 5mm grid while a relatively low temperatures below 300 °C have been predicted by the 10 m grid. A similar trend is shown when $h = 11.27 \, \text{W}/\text{m}^2 \cdot \text{K}$ was used as well, but the sensitivity to the grid size is not very prominent compared to the default model. In addition, the recorded temperatures lower than 400 °C have been predicted for the two finer meshes (2.5 mm and 5 mm).

The heat transfer from the solid surface to its immediate surroundings shows a larger sensitivity to the grid size when, the default CHTM is used and compared to when, $h = 11.27 \, \text{W}/\text{m}^2 \cdot \text{K}$ was used; the predictions show a large deviation in 2.5 mm and 5 mm grids from the 10 mm grid size.

4.2.4   Default CHTM in FDS

As discussed in the previous chapter, the default model for heat convection from a solid surface in FDS uses simplified empirical correlations based on forced, natural convection and pure conduction. In applications where the results produced by this model are of great importance, it is essential to analyse the model performance. Under this section, the steady state performance of the default CHTM in FDS is compared against the hand calculated convective heat transfer coefficient used as a constant in FDS using similar settings. The predictions of both axial plume temperature and $\mathbf{u}_\text{w}$ profiles are analysed in this section.

The constant h (CH-δn) simulations are used here as a benchmark case to evaluate the performance of the default CHTM. The grid size is also a performance indicator for the default CHTM due to the fact that the transfer of heat being modelled as a conduction

problem, if the grid is fine enough to override the other two settings. The axial plume temperature for each cell size is shown below in Fig.4.6.
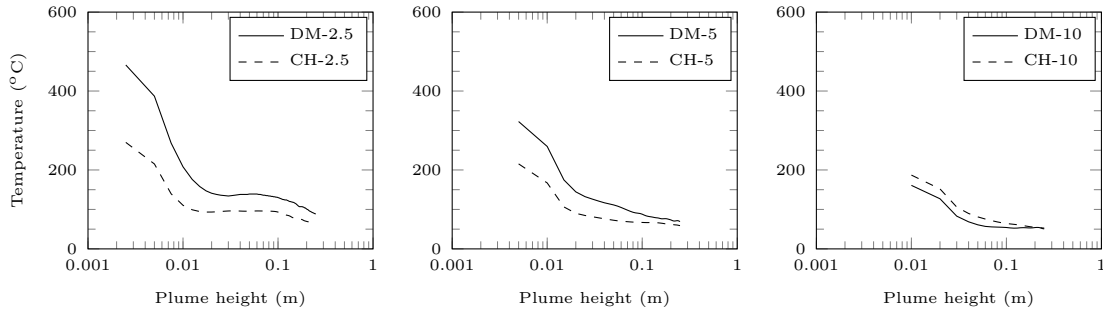
Figure 4.6: Plume Temperature profiles for different δn. Left: $\delta n = 2.5\,\text{mm}$. Middle: $\delta n = 5\,\text{mm}$. Right: $\delta n = 10\,\text{mm}$.

For the coarser grid sizes, $\delta n = 10\,\text{mm}$ and $\delta n = 5\,\text{mm}$, both the default model and constant h calculations have produced results with very little deviation in along the height of the plume. In contrast, for the finest of the grid sizes, the produced results from each model are not in agreement with each other. The deviation is much more prominent in the region very close to the heated surface even though the default model has predicted higher temperatures in the regions above 10 cm plume height as well. This over-prediction of temperature is translated into an over-prediction in $\mathbf{u}_\text{w}$ as well. (See Fig. 4.7)
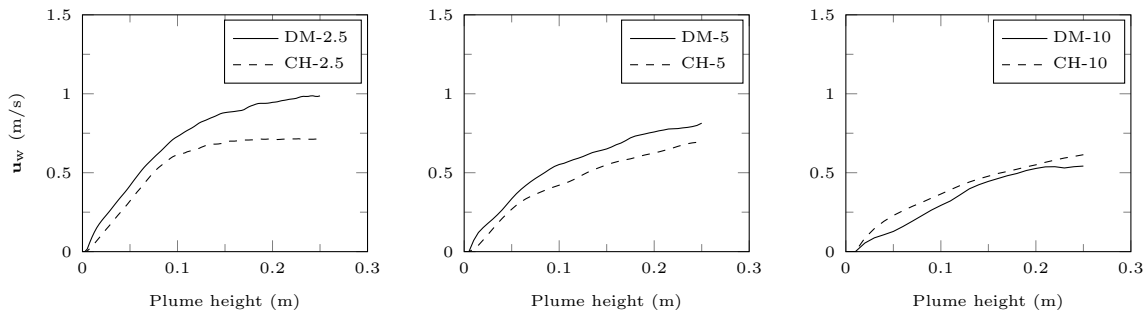
Figure 4.7: $\mathbf{u}_\text{w}$ profiles for different δn. Left: $\delta n = 2.5\,\text{mm}$. Middle: $\delta n = 5\,\text{mm}$. Right: $\delta n = 10\,\text{mm}$.

The focus of this study is mainly on the steady state temperature profiles of the solid phase (Cu plate). The temperature profiles are affected by the water droplets and their interaction with the solid phase. The velocity, droplet temperatures just above the solid surface and the droplet sizes can be considered as critical aspects of the cooling effectiveness of the droplets. The differences in the temperature profiles can be expected to be negligible in steady state even though the difference definitely affects the transient cooling phase and thus, the time to reach the steady states for each case.

4.2.5   Extended Computational Domain

The entrainment of ambient air into the hot rising plume is of great importance, since this phenomena directly affects the energy and mass balance of the plume. The effects of the domain size on the fire plume characteristics has been analysed by Zhang et al. [56]

using the experiments performed by Steckler, Quintiere, and Rinkinen [57]. The focus on
this study [56] has been set on the simulations of fires within closed boundaries using FDS
where, the vent flows through openings have been proven to be sensitive to the domain
size. To be more specific, the inclination of the fire plume has been affected due to the
extension of the domain size. In addition to the domain size used in the earlier subsec-
tions, two more effective extensions of the domain size were considered.

The original domain size was $300\,\text{mm} \times 300\,\text{mm} \times 300\,\text{mm}$. Additionally, the computational
domain was extended to $480\,\text{mm} \times 480\,\text{mm} \times 600\,\text{mm}$ and $600\,\text{mm} \times 600\,\text{mm} \times 600\,\text{mm}$ for
further analysis. The averaged axial velocity and temperature slices of each simulation is
shown below in Fig. 4.8.
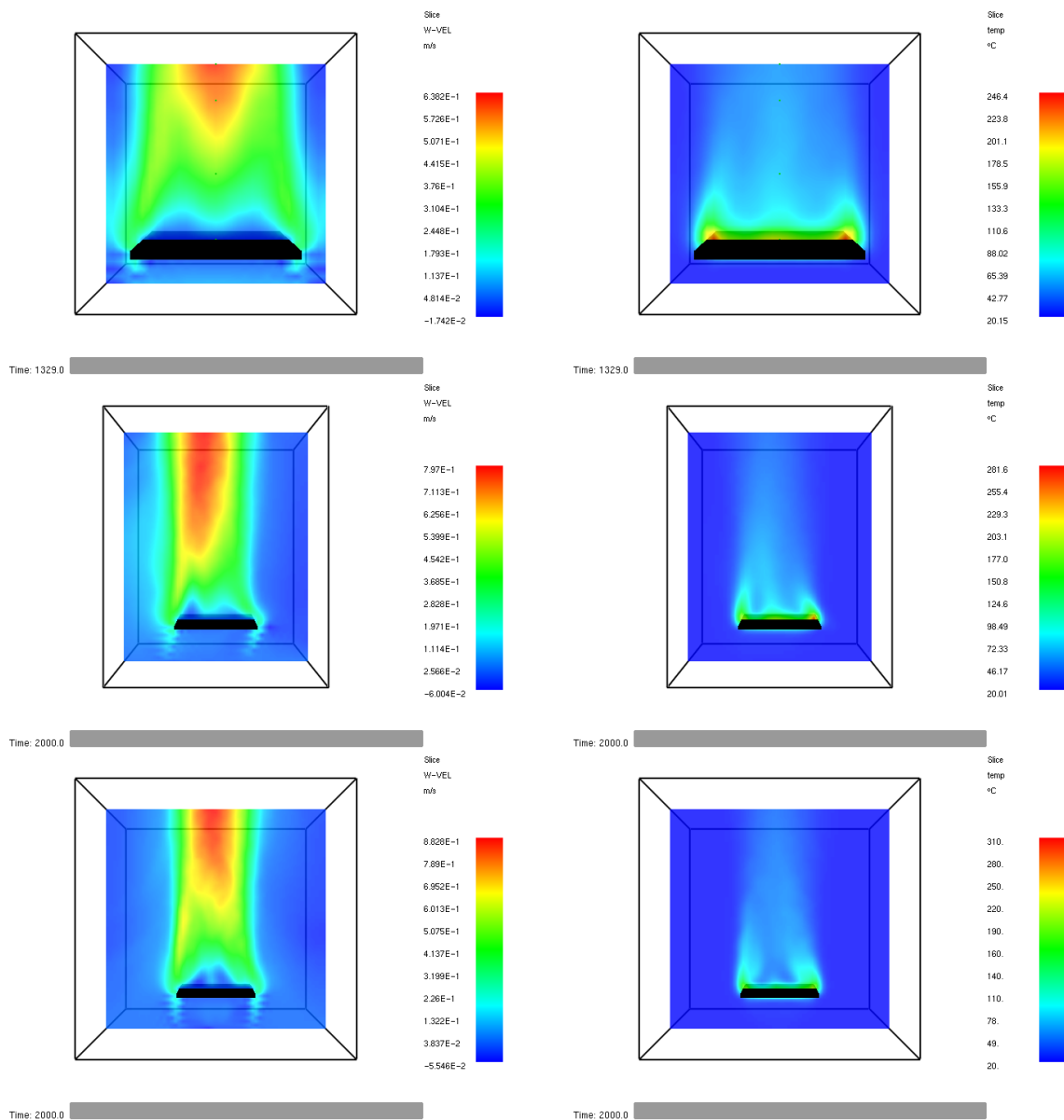
Figure 4.8: Time averaged steady state profiles. Left: Vertical velocity. Right: Plume
temperature. (Top row: Original domain. Middle row: Medium size domain. Bottom
row: Large domain)

The plume axis location is greatly affected by the change of domain dimensions. Con-

sidering that there are no external effects such as wind, a symmetrical plume around the vertical axis was expected. However, symmetrical profiles are not generated in the medium mesh size. For further analysing, a quantitative analysis is provided below. Interestingly, in the larger domain sizes the 'neck' can be observed some distance above the plate.
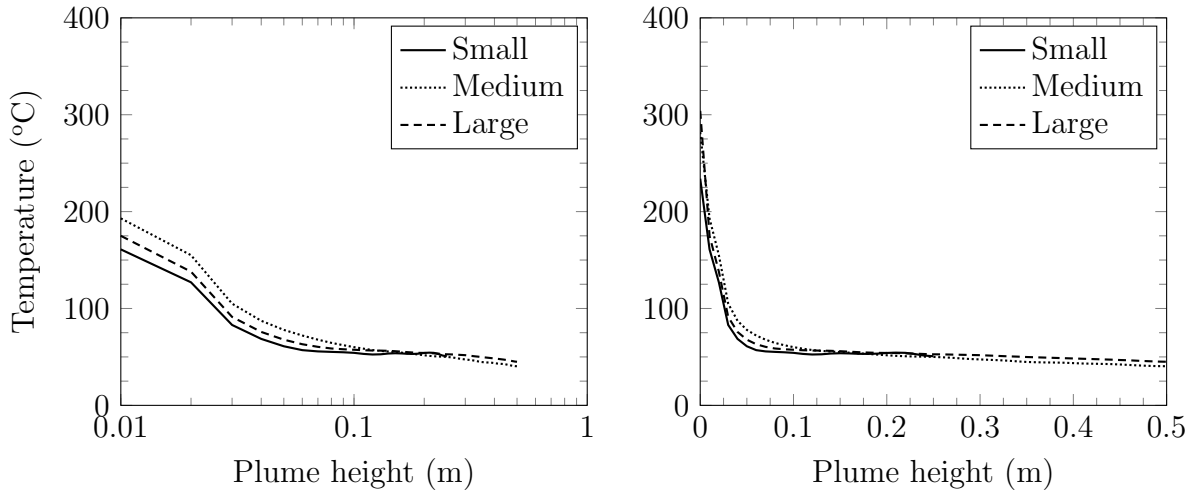
Figure 4.9: Plume temperature profiles for different computational domain dimensions. Left: Log x axis. Right: Normal axes

The near source predictions show a small deviation when the domain size is increased. The near source temperature increases with the size of the domain. Figure 4.9 (Left) highlights this deviation, however, the recorded temperature at $z = 0$ is not available on the same graph. The temperature prediction just above the plate ($z = 0$) in the gas phase has shown a larger variation when the domain size was adjusted. The largest domain predicts a temperature of 304 °C, which was reduced to 282 °C and 234 °C for medium and small domains respectively. Only the near source region seems to be affected by the changes in the domain size while the sensitivity vanishes along the height of the plume.
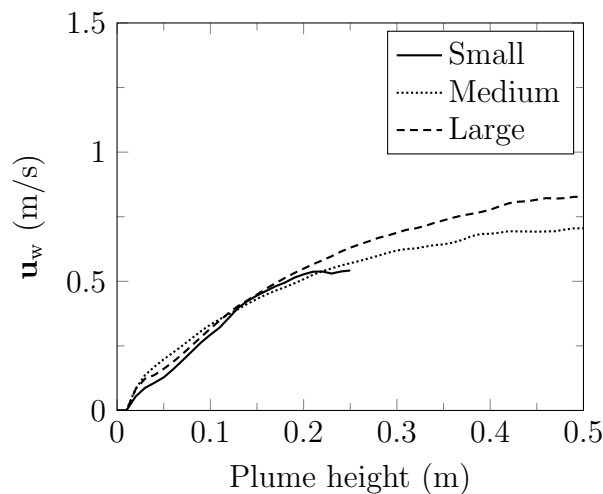
Figure 4.10: $\mathbf{u}_\mathrm{w}$ profiles for different domain sizes

Due to the slight deviations in the temperature predictions in the near source region, similar deviations have been recorded in that region. $\mathbf{u}_w$ has converged for all domain sizes in the region near the position of the water mist nozzle ($z \simeq 0.25\,\text{cm}$).

The effect of the domain size seemed to be negligible in terms of the axial plume temperature profile and also the vertical velocity profile along the axis of the plate. Therefore, going forward from this point onwards the smallest domain size was selected as the appropriate domain dimensions. It should be noted here that at steady conditions after the water spray has been activated the plume temperatures are expected to be lower due to the presence of water droplets in the environment which can further make the effect of the domain size negligible.

Chapter 5

Modelling of the Water Sprays

Due to the missing parameters required to model the water spray including both the nozzle and also the water droplets, simulations including only the water mist nozzle were run to analyse and fine tune the parameters in FDS. This chapter is primarily focused on the said simulations including only the liquid phase.

5.1 Modelling of Water Mist Systems in FDS

Both sprinkler systems and water mist systems are modelled in FDS in a similar manner. The locations of water mist nozzles can be specified under the `DEVC` line along with the properties of the water mist system which are specified on the relevant `PROP` line. The properties of the water particles are specified in the `PART` line which can then be recalled in the `PROP` line.

5.1.1 Water Droplets

The properties of the water droplets that have to be specified in FDS include, the volume median diameter (VMD) of the water spray size distribution, type of the distribution and the convective heat transfer coefficient between the water droplets and the solid surface. The convective heat transfer can be user specified in FDS. There is also the possibility to use a dynamic model which calculates heat transfer coefficient between the two phases.

Volume Median Diameter (VMD)

The size distribution of the spray is characterized by the VMD which can be specified using the `DIAMETER` in micrometers. This diameter represents the point in the distribution where 50% of the water volume is made of droplets having lower diameters than this value.

Particle Size Distribution

The default setting for the particle size distribution in FDS is `ROSIN-RAMMLER-LOGNORMAL` which is, as the name suggests, a combination of lognormal and Rosin-Rammler probability density functions. This can be altered between the two functions as a standalone of each function and there is also the possibility of simulating a mono-disperse spray by adding `MONODISPERSE=.TRUE.` on the `PART` line.

Convective Heat Transfer Coefficient with the Solid Phase

The convective heat transfer with a solid phase is the main focal point in impingement cooling using liquids, in this case water. The convective heat transfer coefficient is calculated using an empirical correlation as explained earlier in section. However, there is also the possibility to specify a constant for this parameter using a positive value for `HEAT_TRANSFER_COEFFICIENT_SOLID`. By setting the same parameter to a negative value, the empirical model can be activated in FDS.

5.1.2   Water Mist Spray

Parameters related to the set-up of the sprays in the simulations are provided below.

Initial Placement of the Droplets

When a water stream or a jet exits a nozzle, the creation of separate water droplets occurs once a certain distance has been travelled by the water stream depending on the nozzle configuration and speed of the water jet. This is also referred to as 'break-up' or 'atomization' of water droplets in the literature [58]. Only beyond this distance from the nozzle, is the water jet completely formed by droplets. In FDS, to mimic this behaviour, the droplets are initially placed at some distance away from the nozzle head location. This distance can be specified in FDS under the syntax `OFFSET` in the `PROP` line for the nozzle. The default setting is 5 cm.

Spray Cone Shape

Different nozzle types are available in the market which produce different types of sprays geometrically. A conical spray pattern can be defined in FDS using the `SPRAY_ANGLE` parameter. Two angles have to specified to define a conical spray, outer and inner angles of the spray cone generated. For solid cone sprays, the inner angle is set to 0°.

Water Flow Rate

The flow rate of water through the nozzle has to be defined in FDS as the parameter `FLOW_RATE` in units of l/ min. The parameter `PARTICLE_VELOCITY` should also be specified in conjunction with the water flow rate which sets the initial velocity of the water droplets once they are injected to the domain.

Angular Distribution of Droplets at the injection boundary

The water droplets can be distributed using the parameter `SPRAY_PATTERN_SHAPE`. This can be changed between the default `GAUSSIAN` or `UNIFORM`. The `GAUSSIAN` setting distributes the droplets following a Gaussian profile while a uniform distribution is produced when `UNIFORM` is used. In the simulation run a Gaussian distribution was chosen due to the more tunable variables that comes with it.

`PARTICLES_PER_SECOND`

The water spray is represented by a certain number of computational droplets in FDS. This number can be increased from it default value of 5000 to produce a spray distributed

among a higher number of computational droplets which can improve the accuracy of the calculations and evaporation patterns of the water droplets.

5.2   Computational Set-Up

All simulations were run using a grid resolution of 10mm on a computational domain of $300 \, \text{mm} \times 300 \, \text{mm} \times 400 \, \text{mm}$ on FDS 6.7.5. The water mist nozzle was placed $150 \, \text{mm}$ ($z = 250 \, \text{mm}$ above the origin) below the top boundary of the domain. The simulation time was set to $110 \, \text{s}$ with a `RAMP` set to the flow rate to reach the desired flow rate in $1 \, \text{s}$. The flow rates were chosen to similar to the experiments [7].

Further details of the water droplets and water mist system are presented in the following subsections.

5.2.1   Water Droplets

In FDS the original size distribution of the water droplets has to prescribed as desired by the user in the form of a cumulative volume fraction (CVF) [59]. For the initial analysis, the sprays were modelled as mono-disperse sprays with a specific median size for each test case.

5.2.2   Setting-Up the Water Mist Systems

In the FDS input files, liquid flow rates of each test case were set to achieve the desired mass flow rate mentioned in the experimental data assuming a water density of $1000 \, \text{kg/m}^3$. The offset at the nozzle was also not defined but was set to be equal to one cell length $(0.01 \, \text{m})$ in FDS. Another parameter which was not defined was the spray angle of the cone produced at the nozzle head. The inner angle for a solid cone spray is $0°$ and the outer angle was adjusted to produce good agreement with the experimental work starting from $30°$ to generate a spray covering the whole plate in all directions from a geometrical point of view. `PARTICLES_PER_SECOND` parameter was set to the default value of 5000 for the initial analysis of water mist sprays.

5.3   Results and Discussion

Under this section, the results for the water spray radial velocity distributions, particle fluxes and Sauter mean diameters (SMD) at different heights are presented and discussed. The experimental measurements regarding the water droplets were obtained using Phase Doppler Particle Analysis (PDPA) method and a similar technique was employed in FDS as well. However, more specific details regarding this set-up were not provided in the literature. Therefore, the radius of the sphere used in the PDPA was set to one cell length $(0.01 \, \text{m})$ in the FDS input file.

5.3.1   Simulations for Water Mass Flow Rate of $0.160 \, \text{g/s}$

Water mist spray set-up with a water mass flow rate of $0.160 \, \text{g/s}$ was also modelled in FDS without the heated copper plate. The results are discussed in the sections below.

The Steady State plate temperature and the particle size distribution 4mm above the plate had been measured for this flow rate in experiments. The initial radial size distribution of the spray was provided as well. The initial radial size distributions in the simulations and the experiments are shown in Fig. 5.1 below.
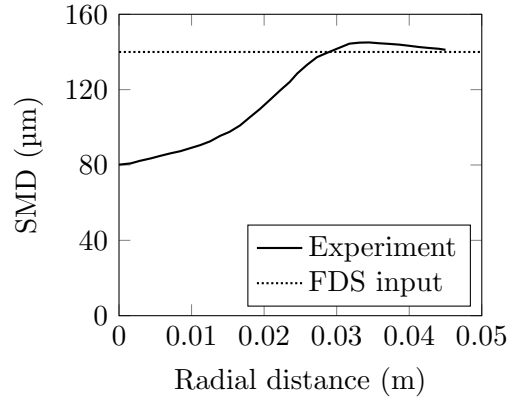

Figure 5.1: Size distributions of the mono-disperse water spray and the experiment. Experimental data was extracted from Fu, Sojka, and Sivathanu (1999) [7].

Here, the mono-disperse spray was assigned a unifor size of 140 µm which was in agreement with a considerable portion of the spray profile measured in the experiments. The selected diameter was the closest resemblance possible while being mono-disperse.

5.3.2   Simulations for Water Mass Flow Rate of 0.385 g/s

In the experimental work different particle size distributions were obtained by altering the operating pressure and the air flow rate through the nozzle. The three particle size distributions from the experiments are shown below in Fig. 5.2 with the size distributions of the corresponding mono-disperse sprays used in the simulations for each size distribution.
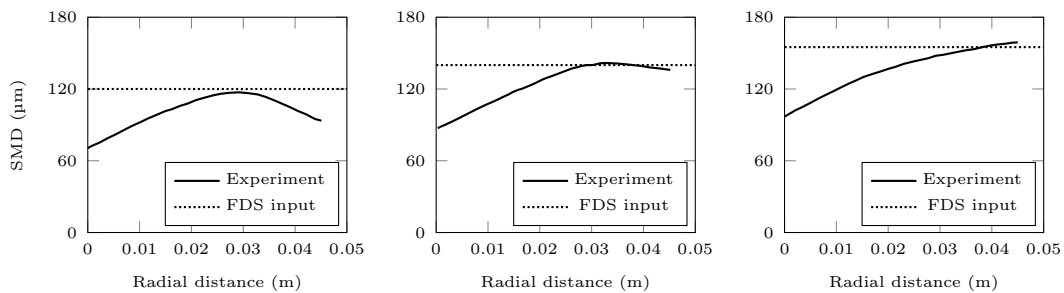
Figure 5.2: Size distributions of the mono-disperse water spray and the experiment for water mass flow rate of 0.385 g/s. Left: Size 1. Middle: Size 2. Right: Size 3. Experimental data extracted from Fu, Sojka, and Sivathanu (1999) [7]

All mono-disperse sprays were characterized, as shown, by the upper limits (120 µm for 'Size 1', 140 µm for 'Size 2' and 155 µm for 'Size 3') of the experimental spray profiles. The upper limit was chosen mainly due to the ease of separating the sprays in terms of the size distributions compared to the less varied lower limit values in the experiments where all the sprays is in range between 70 µm and 100 µm.

In addition to the size distributions of the initial spray, the radial velocity profile of
the initial spray measured 250 mm downstream of the nozzle was also provided in the
literature but only for 'Size 2' which is given below in Fig. 5.3.
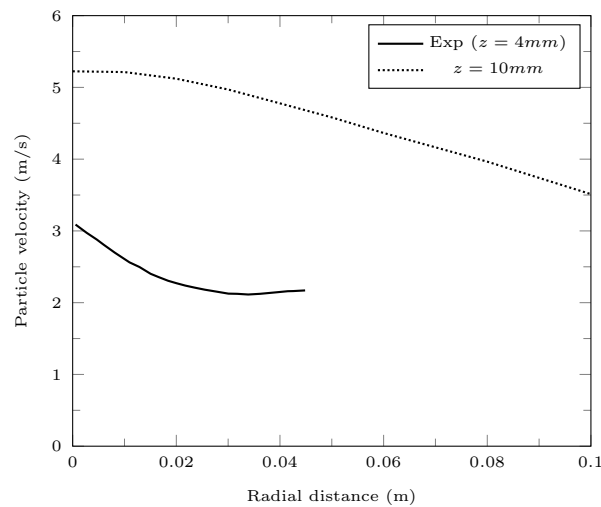
Figure 5.3: Particle velocity (vertical component) of the mono-disperse water spray at
different heights. Experimental data was extracted from Fu, Sojka, and Sivathanu (1999)
[7].

It is mentioned in the experimental work [7] that the velocity distribution was affected by
the droplets size distribution. The mono-disperse spray profile was a uniform distribution
characterised by the upper limit for this spray profile. Therefore, the increased velocities
were expected for this spray due to the absence of smaller droplets in the spray.

The results can certainly be improved if the spray is modelled as a poly-disperse spray
which will then take into account the effects of smaller droplets to the mean values.

Chapter 6

Simulations of the Water and Hot Plate Interaction

This chapter is purely dedicated to the simulations involving the injection of the water droplets to the computational domain. Similar to the previous chapter, the computational set-up and the list of the simulations are presented in the beginning of the chapter which is then followed by the discussion of the results in the form of a comparison between the experimental data [7] and the numerical simulations.

6.1 Computational Set-Up

Simulations including the whole set-up from the experiments were run after analysing the results of each individual phase discussed in the previous two chapters. The modelling of the water spray was not straightforward due to the unavailability of major input data for the simulations related to the water mist system and water droplets. Therefore, the simulations with mono-disperse sprays were considered for simplicity and ease of analysing the results afterwards.

6.1.1 Simulations with a Mono-Disperse Spray

As discussed in the earlier chapter, a mono-disperse spray profile was used for the simulations initially before moving onto poly-disperse sprays. The computational domain was similar to that mentioned in the solid phase only simulations. The settings related to the solid phase (Cu plate) discussed in the same chapter were also used for these simulation without any changes. The same can be said about the water mist system set-up where similar settings for the mono-disperse sprays from the previous chapter were used. The grid cell size was set to 10 mm for all simulations discussed under this chapter.

The computational time was set to 4500 s and the water was introduced at exactly 1999.0s which was kept active until the end of simulations. The setting of 4500 s allowed to achieve a steady state of approximately 500 s long after the water mist system was activated. Unlike in the previous simulations without water droplets, to speed the calculations up in FDS, the `TIME_SHRINK_FACTOR` was not set for any of the simulations discussed in this chapter.

6.2 Results and Discussion

The discussion of the results is focused mainly on the steady state plate temperature for the different flow rates used and the different size distributions used in the experiments. Simulations were run using mono-disperse spray profiles and poly-disperse profiles.

6.2.1 Simulations for 0.160 g/s Water Flow Rate

Initially an assumption was made on both the `PARTICLE_VELOCITY` and outer angle of the spray cone to be $20\,\mathrm{m/s}$ and $30°$ respectively. The experimental model in FDS was activated while the droplet movement on the solid surface was set to its default setting, `HORIZONTAL_VELOCITY=0.2` ($HV = 0.2\,\mathrm{m/s}$). According to the observations made in the experiment, the water droplets reached the surface at rather low droplet sizes with the smaller droplets evaporating without even making it to the surface. Regarding the droplets sizes in the mono-disperse spray, a spray with a volume median diameter (VMD) of $140\,\mathrm{\mu m}$ selected to represent the largest possible droplets which presents the most cooling potential with respect to the droplet sizes. The idea was to reach as close to the experimental data as possible by altering many other undefined parameters while keeping this setting at the most favourable position.

Simulations with different settings were run in order to capture the effects of each of these parameters. Table 6.1 below summarises all the different settings used for each simulation with a specific ID.

Table 6.1: Settings of simulations with a water flow rate of $0.160\,\mathrm{g/s}$.

Simulation ID	HORIZONTAL_VELOCITY	HEAT_TRANSFER_– COEFFCIENT_SOLID
$HV = 0.2\,\mathrm{m/s}$	0.2	-1
$HV = 0\,\mathrm{m/s}$	0	-1
$h_w = 300\,\mathrm{W/\,(m^2 \cdot K)}$	0.2	300
$h_w = 150\,\mathrm{W/\,(m^2 \cdot K)}$	0.2	150

The steady state plate temperature profile from the experiments for this case is plotted with the results from the simulations in Fig. 6.1 below.
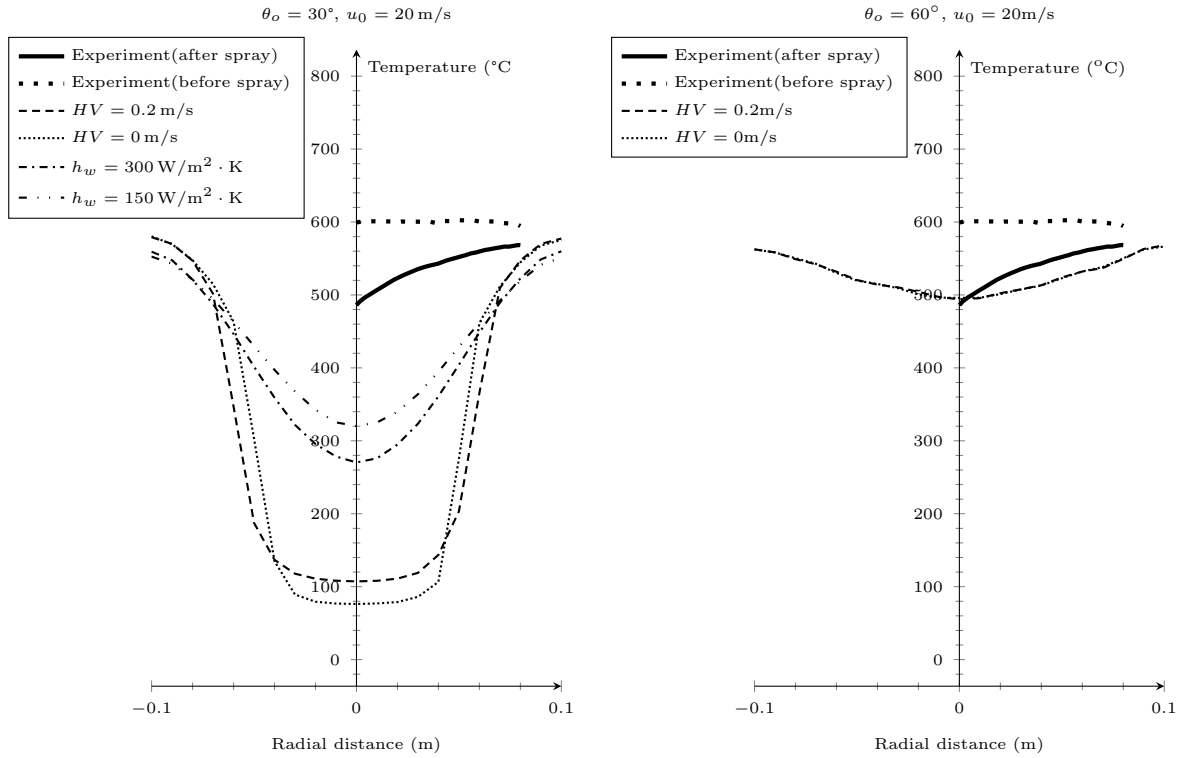
Figure 6.1: Steady state radial temperature profile of the plate for different θ_o with a water mass flow rate of $0.160\,\text{g/s}$ and $u_0 = 20\,\text{m/s}$. Left: $\theta_o = 30°$. Right: $\theta_o = 60°$. Experimental data was extracted from Fu, Sojka, and Sivathanu (1999) [7].

θ_o when set to 30° caused almost all of the water droplets to fall onto the heated surface which resulted in more heat being absorbed from the surface compared to the experiments. It was quite clear that the amount of heat absorbed by the water droplets had to be further reduced to achieve better agreement to the experimental data. This was also confirmed by the fact that even when the h_w was reduced further to $300\,\text{W/m}^2 \cdot \text{K}$ and to $150\,\text{W/m}^2 \cdot \text{K}$. If this amount of water droplets hit the surface at this flow rate the convective heat transfer coefficient should be lower than even $150\,\text{W/m}^2 \cdot \text{K}$ which is not realistic and far too low for water spray impingement cooling (See Fig. 1.1.).

In order to reduce the heat absorbed by the water droplets θ_o was doubled so that only a portion of the water droplets were directly impinging on the heated surface while the rest of the droplets were interacting directly only with the rising plume. After this adjustment of θ_o, much better agreement was shown by the simulations using the experimental model implemented in FDS 6.7.5. After the water mist settings seems to be somewhat sorted out, the properties of water droplets were adjusted to achieve even better agreement and also to perform an analysis on the effects of a poly-disperse spray profile. A poly-disperse spray profile can be modelled in number of ways in FDS. Further details about the poly-disperse simulations are discussed along with the results from the simulation below.

It was also noted that the effect of the HV parameter was also negligible when the spray angle was changed to 60° due to the number of droplets impinging on the plate is much lower compared to that of the smaller θ_o.

Poly-Disperse Simulations

All the settings of the were kept unchanged while the spray was made a poly-disperse one by removing `MONODISPERSE=.TRUE.` from the `PART` line foe the water droplets. The default distribution for water droplet size is `ROSIN-RAMMLER-LOGNORMAL` with a default width of `GAMMA_D=2.4` ($\gamma = 2.4$). These settings were also unchanged for the initial analysis. For poly-disperse spray profiles the parameter `PARTICLES_PER_SECOND` is very vital for both computational efficiency and also accuracy of the calculations performed. This was set to `PARTICLES_PER_SECOND=5000` to begin with. A sensitivity analysis was performed for this parameter as well.

The steady state plate temperature profile for the above settings are shown below in Fig. for different widths of the `ROSIN-RAMMLER-LOGNORMAL` function (γ) used for the poly-disperse spray. This parameter was specified in the `PART` line for water droplets using the syntax `GAMMA_D` in the input file. The default setting in FDS 6.7.5 is `GAMMA_D=2.4`.
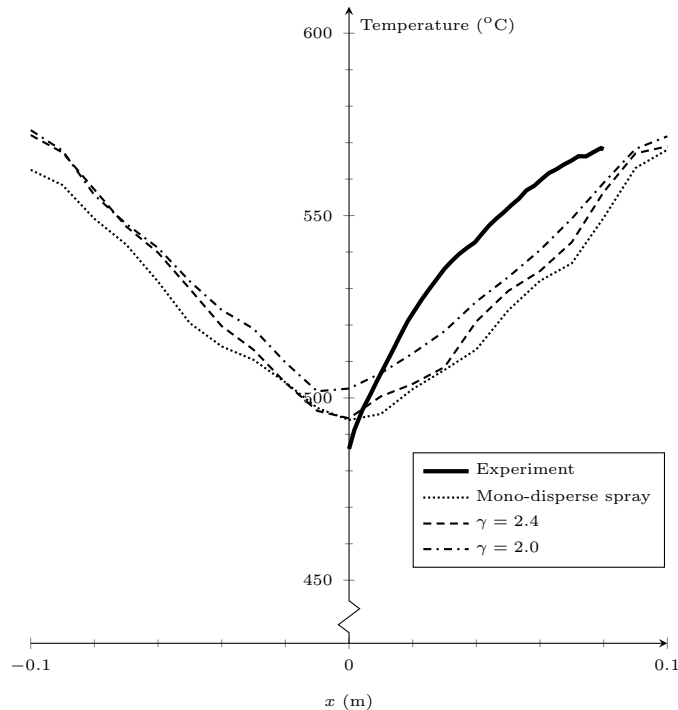
Figure 6.2: Steady state plate temperature profiles for flow rate of 0.160 g/s. Experimental data was extracted from Fu, Sojka, and Sivathanu (1999) [7].

The effect of the spray profile in the poly-disperse spray profile affected not only the minimum temperature recorded at the center of the plate, but also the shape of the temperature profile by making the reading away from the center moving to a better agreement.

6.2.2   Simulations for 0.385 g/s Water Flow Rate

As explained in earlier chapters, the water mass flow rate was altered in the experiments among 0.160 g/s, 0.385 g/s and 0.600 g/s. This section is wholly focused on the simulations performed for the water mass flow rate of 0.385 g/s.

Three different size distributions for the water spray were used in the experiments by Fu, Sojka, and Sivathanu while maintaining the water flow rate constant at $0.385\,\text{g/s}$. The experimental data and the simulated data for the three size distributions are shown below in Fig. 6.3.

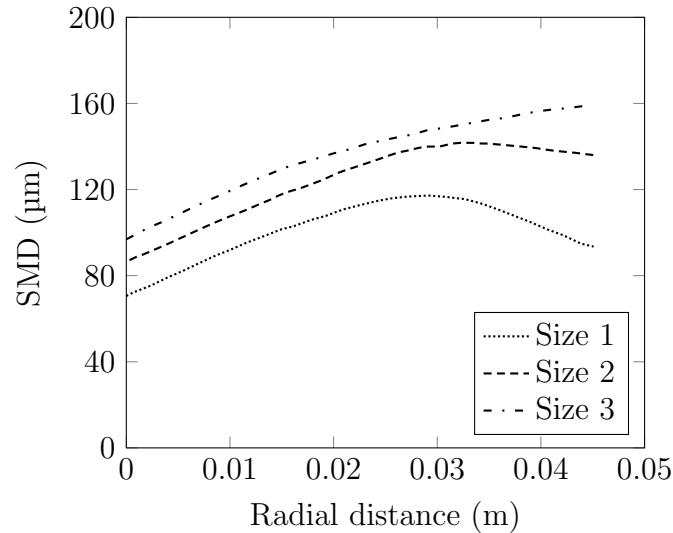Figure 6.3: Size distributions of the mono-disperse water spray and the experiment. Experimental data was extracted from Fu, Sojka, and Sivathanu (1999) [7].

The discussion for this flow rate setting is divided based on these three size distributions which are referred to as 'size 1', 'size 2' and 'size 3' as shown in Fig. 6.3.

Size 1 - Mono-Disperse Simulations

Similar to the above section the mono-disperse spray profile was characterized by the maximum SMD recorded in the experiments. Therefore, size 1 was represented by a mono-disperse spray profile with a droplet diameter with $120\,\mu\text{m}$. The outer angle of the solid cone spray (θ_o) was set to 65° with a particle injection velocity of $25\,\text{m/s}$. The OFFSET parameter was set to $10\,\text{mm}$ to represent one cell thickness from the nozzle head. It should be noted that these parameters were assumed to achieve good agreement with the experimental data due to the lack of these parameters mentioned in the literature. Figure below shows the steady state plate temperature profile in the radial direction both in the experiment and the simulations run with above settings.
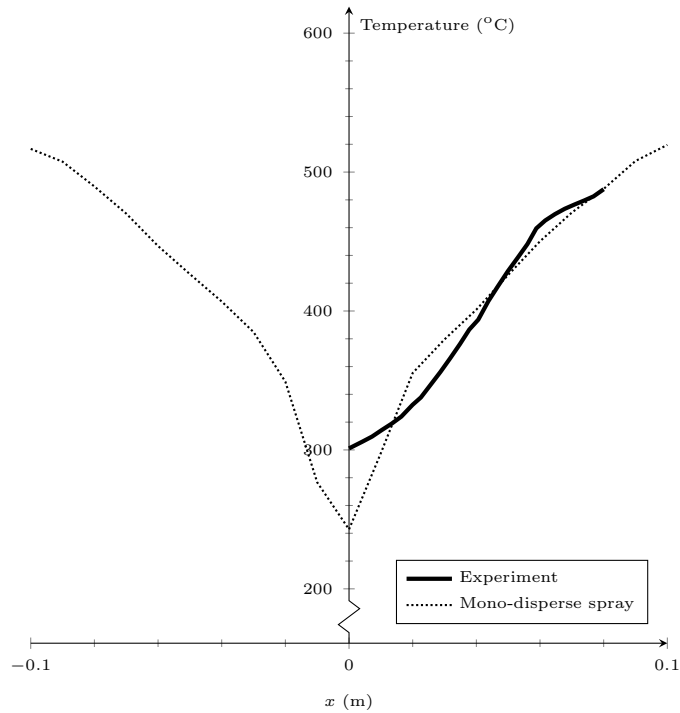
Figure 6.4: Steady state plate temperature profile for particle size distribution 'size 1' in Fig. 6.3. Experimental data was extracted from Fu, Sojka, and Sivathanu (1999.) [7]

The mono-disperse simulation with the assumed settings showed great agreement with the results from the experiments from $0.03\,\mathrm{m}$ away from the center of the plate. Despite the good agreement in that region, the temperatures recorded closer to the center of the plate were significantly higher in the experiments. This was due to the mono-disperse profile containing a uniform SMD of $120\,\mathrm{\mu m}$ across the radial span. The region where the SMD value converges with the experiments is in the region around $0.03\,\mathrm{m}$ away from the center where the maximum SMD of around $120\,\mathrm{\mu m}$ was reached in the experiments. In order to achieve accurate predictions over the whole radial distance, it is expected incorporating a poly-disperse spray matching the experiments will definitely be beneficial.

Size 2 - Mono-disperse Simulations

Keeping all the settings the same, while only changing the particle injection velocity to $20\,\mathrm{m/s}$ and the mono-disperse spray size to $140\,\mathrm{\mu m}$. As per the explanation provided in the experimental work, the different size distributions were obtained varying the operating pressure and the air flow rates through the nozzle. It is also mentioned in the literature that smaller size distributions were associated with higher velocities. This led to keeping the all settings constant from earlier size distribution except for the two parameters mentioned.

Below, in Fig. 6.5, the steady state plate temperature profile from the simulation is plotted and compared with the experimental results.
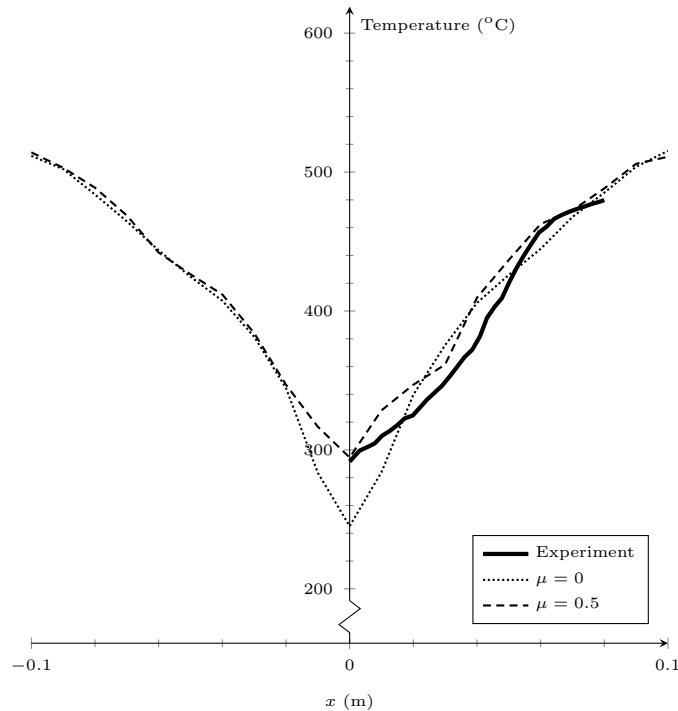
Figure 6.5: Steady state plate temperature profile for particle size distribution 'size 2' in Fig. 6.3. ($\mu = $ SPARY_PATTERN_MU). Experimental data was extracted from Fu, Sojka, and Sivathanu (1999) [7].

Similar to the earlier size distribution, the agreement with the experimental results improved greatly starting from the 0.03 m mark and away from it. The median size used in the mono-disperse spray matched better in this region compared to the region closer to the center of the plate. Due to the droplets having larger diameters in the simulation, in the central region, the cooling was much higher in the simulation compared to the experiments.

To make the minimum temperature recorded at the center of plate move into better agreement, the GAUSSIAN spray profile was altered such that less number of droplets are placed near the center of the plate using the SPRAY_PATTERN_MU parameter (μ). This parameter was changed to 0.5 from its default value of 0 for full cone sprays. As expected, the change in the spacial distribution of water droplets showed better agreement with the experimental results throughout the radius of the plate.

Size 3 - Mono-Disperse Simulations

Following the same procedure as the two earlier test cases, simulations were run with a solid cone spray with $\theta_o = 65°$, particle injection velocity $u_0 = 10$ m/s and a VMD of 155 µm. Good agreement was achieved with these settings against the experimental work as shown below in Fig. 6.6.
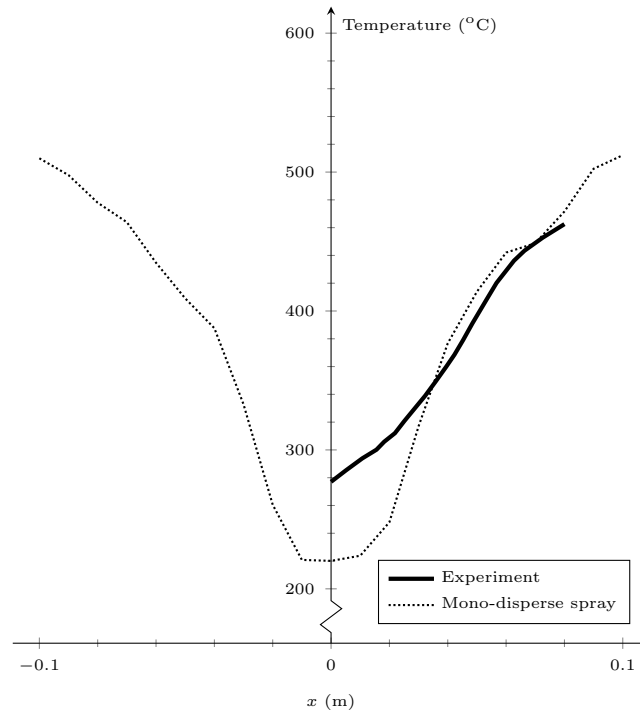
Figure 6.6: Steady state plate temperature profile for particle size distribution 'size 3' in Fig. 6.3. Experimental data was extracted from Fu, Sojka, and Sivathanu (1999) [7].

Again, due to the the mono-disperse spray being characterized by the maximum in the radial size distribution in the experiments, lower temperatures were recorded in near the center of the plate in simulations.

As per the results discussed above, it can be concluded that FDS is very much capable of producing good results at moderate flow rates even though, the predictions for 0.160 g/s case require more adjustments to show further improvement when compared with the experimental results. As shown for the 'Size 2' case, better agreement can be achieved by altering the default SPRAY_PATTERN_SHAPE using the SPRAY_PATTERN_MU AND SPRAY_PATTERN_BETA parameters. The effects of poly-disperse profile was also identified for the test case with flow rate of 0.160 g/s where the recorded temperatures away from the center showed an improvement with the agreement between the simulations and the experiment. However, for poly-disperse simulations, it is essential that the spray matches the provided size distributions in the literature.

Chapter 7

Conclusions and Future Work

Conclusions

The motivation of the thesis was to perform a validation study for FDS on the water spray impingement cooling of hot surfaces with large super heats resembling a flaming surface. Fu, Sojka, and Sivathanu [7] performed experiments using a superheated Cu plate at 600 °C which was then cooled down using a water mist system with different settings. The steady state measurements were obtained for plate temperature, size and velocity distributions for different water flow rates at different locations for different velocity and size profiles. The experimental set-up was modelled in FDS version 6.7.5 with minor adjustments such as using a square shaped Cu plate instead of a round plate similar to the experiment.

The simulations were performed in a series of different steps starting with only the solid phase and the gas phases before moving on to the introduction of water droplets to the domain. The motive of this approach was to assess the performance of FDS in providing accurate prediction in the buoyant 'lazy' plume rising from the heated surface. There were no such analysis on the plume properties performed in the experimental work in focus [7], therefore, a separate set of experiments were chosen in order to simulate the lazy plume and compare FDS results. The results for the default CHTM seems to agree with the experimental work when a fine mesh resolution was used. Instead of the default model for heat convection in FDS, a specified constant heat transfer coefficient was also used for comparison purposes. The specified value was obtained from simple hand calculations. There seemed to be some notable difference between the two models in the steady state predictions of axial plume temperature and the vertical velocity component, more notably as the grid resolution became higher.

Many of the key parameters related to the water mist system was not documented by the authors in their work [7]. This led to making assumptions for these missing parameters in the hopes of achieving proper agreement with the experimental work. To make the situation less complicated mono-disperse spray profiles were used in the simulations to minimize the variables associated with guessing. Out of the total 5 different experiments performed in the experiments, reasonable agreement was achieved with four test cases using only a mono-disperse profile and a coarse mesh. Further fine tuning the spray properties led to even better agreement in one specific case ('Size 2' case with flow rate set to 0.385 g/s).

All the work presented highlighted the importance of modelling the water mist spray in FDS. Even with mono-disperse sprays, the temperature profiles similar to the experiments were achieved in numerical simulations by adjusting the unknowns.

Future Work

The results from the simulations justified the capabilities of FDS to predict the interaction between the two phases (Three, if you include the gas phase as well). All these simulations employed a mono-disperse profile for the water droplet size distribution and the next step is identified as moving forward with the poly-disperse sprays for all test cases and complete the validation study. The velocity and size distributions of the experiments at steady conditions was also provided which tests the predictions related with the interaction of the water droplets with gas phase as well. The poly-disperse profile is required to compare the results with these data from experiments further emphasizing on the importance of the poly-disperse spray simulations. The effort made here provides a foundation to build upon and reaching the completion of the validation study.

Acknowledgements

Bibliography

[1] V. Novozhilov et al. "A computational fluid dynamics study of wood fire extinguishment by water sprinkler". In: *Fire Safety Journal* 29.4 (1997), pp. 259–282. ISSN: 0379-7112. DOI: https://doi.org/10.1016/S0379-7112(97)00027-1.

[2] Durga Ghosh et al. "Impingement Cooling of Hot Metal Strips in Runout Table-A Review". In: *Interfacial Phenomena and Heat Transfer* 3 (2 Jan. 2015). DOI: 10.1615/InterfacPhenomHeatTransfer.2014010574.

[3] S. D. Cox, S. J. Hardy, and D. J. Parker. "Influence of runout table operation setup on hot strip quality, subject to initial strip condition: Heat transfer issues". In: *Ironmaking and Steelmaking* 28 (Oct. 2001), pp. 363–372. DOI: 10.1179/030192301678226.

[4] P. Bhattacharya, A. N. Samanta, and S. Chakraborty. "Spray evaporative cooling to achieve ultra fast cooling in runout table". In: *International Journal of Thermal Sciences* 48.9 (2009), pp. 1741–1747. ISSN: 1290-0729. DOI: https://doi.org/10.1016/j.ijthermalsci.2009.01.015.

[5] M. H. Shi, T. C. Bai, and J. Yu. "Dynamic behavior and heat transfer of a liquid droplet impinging on a solid surface". In: *Experimental Thermal and Fluid Science* 6.2 (1993), pp. 202–207. ISSN: 0894-1777. DOI: https://doi.org/10.1016/0894-1777(93)90030-M.

[6] Lanchao Lin and Rengasamy Ponnappan. "Heat Transfer Characteristics of Evaporative Spray Cooling in a Closed Loop". In: *SAE Transactions* 111 (2002), pp. 756–764. ISSN: 0096736X, 25771531. URL: http://www.jstor.org/stable/44718485.

[7] Chunming Fu, Paul E. Sojka, and Yudaya R. Sivathanu. "On the Interaction Between Evaporating Sprays and Heated Surfaces". In: *Proceedings of the 12th annual conference on liquidatomization and spray systems,* 1999. eprint: https://www.nist.gov/document/fu-interaction-between-evaporating-sprays-and-heated-surfacespdf.

[8] Martin Rein. "Interactions between Drops and Hot Surfaces". In: *Drop-Surface Interactions.* Ed. by Martin Rein. Vienna: Springer Vienna, 2002, pp. 185–217. ISBN: 978-3-7091-2594-6. DOI: https://doi.org/10.1007/978-3-7091-2594-6_6.

[9] M. di Marzo and D. D. Evans. "Evaporation of a water droplet deposited on a hot high thermal conductivity solid surface". In: (Aug. 1986). URL: https://www.osti.gov/biblio/7111206.

[10] Bohumil Horacek, Kenneth T. Kiger, and Jungho Kim. "Single nozzle spray cooling heat transfer mechanisms". In: *International Journal of Heat and Mass Transfer* 48.8 (2005), pp. 1425–1438. ISSN: 0017-9310. DOI: `https://doi.org/10.1016/j.ijheatmasstransfer.2004.10.026`.

[11] Santosh Kumar Nayak, Purna Chandra Mishra, and Sujay Kumar Singh Parashar. "Influence of spray characteristics on heat flux in dual phase spray impingement cooling of hot surface". In: *Alexandria Engineering Journal* 55.3 (2016), pp. 1995–2004. ISSN: 1110-0168. DOI: `https://doi.org/10.1016/j.aej.2016.07.015`.

[12] Donald E. Tilton, Martin R. Pais, and Louis C. Chow. *High power density spray cooling*. Tech. rep. University of Kentucky, Dept of Mechanical Engineering, Lexington, 1989. URL: `https://apps.dtic.mil/sti/pdfs/ADA213575.pdf`.

[13] Zhigang Liu and Andrew K. Kim. "A Review of Water Mist Fire Suppression Systems— Fundamental Studies". In: *Journal of Fire Protection Engineering* 10.3 (1999), pp. 32–50. DOI: `10.1177/104239159901000303`.

[14] Wilhelm Schmidt. "Turbulente Ausbreitung eines Stromes erhitzter Luft". In: *ZAMM - Journal of Applied Mathematics and Mechanics / Zeitschrift für Angewandte Mathematik und Mechanik* 21.6 (1941), pp. 351–363. DOI: `https://doi.org/10.1002/zamm.19410210603`.

[15] Hunter Rouse, C. S. Yih, and H. W. Humphreys. "Gravitational Convection from a Boundary Source". In: *Tellus* 4.3 (1952), pp. 201–210. DOI: `https://doi.org/10.1111/j.2153-3490.1952.tb01005.x`.

[16] B. R. Morton, Geoffrey Taylor Ingram, and John Stewart Turner. "Turbulent gravitational convection from maintained and instantaneous sources". In: *Proceedings of the Royal Society of London. Series A. Mathematical and Physical Sciences* 234.1196 (1956), pp. 1–23. DOI: `10.1098/rspa.1956.0011`.

[17] G. K. Batchelor. "Heat convection and buoyancy effects in fluids". In: *Quarterly Journal of the Royal Meteorological Society* 80.345 (1954), pp. 339–358. DOI: `https://doi.org/10.1002/qj.49708034504`.

[18] Chia-Shun Yih. "Free Convection Due to a Point Source of Heat". In: *Selected Papers by Chia-Shun Yih*. 1951, pp. 734–740. DOI: `10.1142/9789812813084_0065`.

[19] B. R. Morton. "Forced plumes". In: *Journal of Fluid Mechanics* 5.1 (1959), pp. 151–163. DOI: `10.1017/S002211205900012X`.

[20] B. R. Morton and Jason Middleton. "Scale diagrams for forced plumes". In: *Journal of Fluid Mechanics* 58.1 (1973), pp. 165–176. DOI: `10.1017/S002211207300220X`.

[21] G. R. Hunt and N. B. Kaye. "Lazy plumes". In: *Journal of Fluid Mechanics* 533 (2005), pp. 329–338. DOI: `10.1017/S002211200500457X`.

[22] Ali Tohidi and Nigel B. Kaye. "Highly buoyant bent-over plumes in a boundary layer". In: *Atmospheric Environment* 131 (2016), pp. 97–114. ISSN: 1352-2310. DOI: `https://doi.org/10.1016/j.atmosenv.2016.01.046`.

[23] K. Tory. *Models of buoyant plume rise*. Research rep. Bushfire and Natural Hazards CRC, Dec. 18, 2018. URL: `https://www.bnhcrc.com.au/file/9385/download?token=KyzcAEL3`.

[24] T. K. Fanneløp and D. M. Webber. "On buoyant plumes rising from area sources in a calm environment". In: *Journal of Fluid Mechanics* 497 (2003), pp. 319–334. DOI: `10.1017/S0022112003006669`.

[25] Xin Wang et al. "Particle image velocimetry investigation on air distribution of surface-source buoyancy plume changing heating intensity and structure size in a thermostatic chamber". In: *Indoor and Built Environment* (May 20, 2020). DOI: `10.1177/1420326X20926245`.

[26] P. Carlotti and G. R. Hunt. "An entrainment model for lazy turbulent plumes". In: *Journal of Fluid Mechanics* 811 (2017), pp. 682–700. DOI: `10.1017/jfm.2016.714`.

[27] Brian D. Landers, P. Disimile, and N. Toy. "The fluid thermal field over a flat heated disk". In: *International Journal of Heat and Technology* 35 (2017), pp. 799–805. ISSN: 0392-8764. DOI: `10.18280/ijht.350415`.

[28] Frederic Plourde et al. "Direct numerical simulations of a rapidly expanding thermal plume: structure and entrainment interaction". In: *Journal of Fluid Mechanics* 604 (Jan. 2008), pp. 99–123. DOI: `10.1017/S0022112008001006`.

[29] Gordon Taub et al. "An examination of the high-order statistics of developing jets, lazy and forced plumes at various axial distances from their source". In: *Journal of Turbulence* 16 (Sept. 2015). DOI: `10.1080/14685248.2015.1008006`.

[30] David Hargreaves, Matthew Scase, and Iona Evans. "A simplified computational analysis of turbulent plumes and jets". In: *Environmental Fluid Mechanics* 12 (Dec. 2012), pp. 555–578. DOI: `10.1007/s10652-012-9250-7`.

[31] National Board of Fire Underwriters and Underwriters' Laboratories. *The Mechanism of Extinguishment of Fire by Finely Divided Water: An Investigation*. NBFU research report. National Board of Fire Underwriters, Committee on Fire Prevention and Engineering Standards, Research Division, 1955.

[32] D. J. Rasbash and Z. W. Rogowski. "Extinction of fires in liquids by cooling with water sprays". In: *Combustion and Flame* 1.4 (1957), pp. 453–466. ISSN: 0010-2180. DOI: `https://doi.org/10.1016/0010-2180(57)90006-8`.

[33] D. J. Rasbash, Z. W. Rogowski, and G. W. V. Stark. "Mechanisms of extinction of liquid fires with water sprays". In: *Combustion and Flame* 4 (1960), pp. 223–234. ISSN: 0010-2180. DOI: `https://doi.org/10.1016/S0010-2180(60)80026-0`.

[34] Francesco Tamanini. "The Application of Water Sprays to the Extinguishment of Crib Fires". In: *Combustion Science and Technology* 14.1-3 (1976), pp. 17–23. DOI: `10.1080/00102207608946742`.

[35] Richard S. Magee and Rolf D. Reitz. "Extinguishment of radiation augmented plastic fires by water sprays". In: *Symposium (International) on Combustion* 15.1 (1975). Fifteenth Symposium (International) on Combustion, pp. 337–347. ISSN: 0082-0784. DOI: `https://doi.org/10.1016/S0082-0784(75)80309-2`.

[36] Zhigang Liu and Andrew K. Kim. "A Review of Water Mist Fire Suppression Systems— Fundamental Studies". In: *Journal of Fire Protection Engineering* 10.3 (1999), pp. 32–50. DOI: `10.1177/104239159901000303`.

[37] G. Grant, J. Brenton, and D. Drysdale. "Fire suppression by water sprays". In: *Progress in Energy and Combustion Science* 26.2 (2000), pp. 79–130. ISSN: 0360-1285. DOI: `https://doi.org/10.1016/S0360-1285(99)00012-X`.

[38] J. R. Mawhinney and J. K. Richardson. "A review of water mist fire suppression research and development, 1996". In: *Fire Technology* 33.1 (1997), pp. 54–90. DOI: `https://doi.org/10.1023/A:1015322428719`.

[39] J. R. Mawhinney, B. Z. Dlugogorski, and A. K. Kim. "A closer look at the fire extinguishing properties of water mist". In: *Fire Safety Science* 4 (1994), pp. 47–60.

[40] A. E. Cote et al. *Fire Protection Handbook*. Fire Protection Handbook v. 2. National Fire Protection Association, 2008. ISBN: 9780877657583. URL: `https://books.google.be/books?id=e2eWA9d2a8IC`.

[41] Ragnar Wighus. "Extinguishment Of Enclosed Gas Fires With Water Spray". In: *Fire Safety Science* 3 (Jan. 1991), pp. 997–1006. DOI: `10.3801/IAFSS.FSS.3-997`.

[42] Joachim Søreng Bjørge et al. "Method for Measuring Cooling Efficiency of Water Droplets Impinging onto Hot Metal Discs". In: *Applied Sciences* 8.6 (2018). ISSN: 2076-3417. DOI: `10.3390/app8060953`.

[43] Eric Link et al. "Measurements of spray-plume interactions for model validation". In: *Fire Safety Journal* 91 (2017). Fire Safety Science: Proceedings of the 12th International Symposium, pp. 714–722. ISSN: 0379-7112. DOI: `https://doi.org/10.1016/j.firesaf.2017.04.024`.

[44] Tarek Beji et al. "Numerical modelling of the interaction between water sprays and hot air jets - Part II: Two-phase flow simulations". In: *Fire Safety Journal* 96 (2018), pp. 143–152. ISSN: 0379-7112. DOI: `https://doi.org/10.1016/j.firesaf.2018.01.006`.

[45] M. Faghri and Bengt Sundén. *Transport Phenomena in Fires*. English. Developments in Heat Transfer, United Kingdom: WIT Press, 2007. ISBN: 978-184564-160-3.

[46] N. Johansson and M. Ekholm. "Variation in Results Due to User Effects in a Simulation with FDS". In: *Fire Technology* 54 (1 2018), pp. 97–116. ISSN: 1572-8099. DOI: `10.1007/s10694-017-0674-y`.

[47] Kevin McGrattan et al. "Fire dynamics simulator, user's guide". In: *NIST special publication 1019* 1019.6 (Mar. 9, 2020). eprint: `https://github.com/firemodels/fds/releases/download/FDS6.7.4/FDS_User_Guide.pdf`.

[48] Engineering ToolBox. *Emissivity Coefficient Materials*. 2003. URL: `https://www.engineeringtoolbox.com/emissivity-coefficients-d_447.html`.

[49] Dougal Drysdale. "Heat Transfer". In: *An Introduction to Fire Dynamics*. John Wiley and Sons, Ltd. Chap. 2, pp. 35–82. ISBN: 9781119975465. DOI: `https://doi.org/10.1002/9781119975465.ch2`.

[50] Jack P. Holman. *Heat transfer*. Ed. by Jack P. Holman and John Lloyd. 10th ed. McGraw-Hill, 2010. ISBN: 978-0-07-352936-3.

[51] Theodore. L. Bergman et al. *Fundamentals of Heat and Mass Transfer*. Ed. by Linda Ratts. 7th ed. John Wiley and Sons, 2007. ISBN: 978-0470-50197-9.

[52] Peter Veloo and James Quintiere. "Convective heat transfer coefficient in compartment fires". In: *Journal of Fire Sciences* 31 (Aug. 2013), pp. 410–423. DOI: `10.1177/0734904113479001`.

[53] AZoM. *Stainless Steel - Grade 316 (UNS S31600)*. AZoNetworks. Sept. 13, 2001. URL: `https://www.azom.com/article.aspx?ArticleID=863`.

[54] Calex Electronics Limited. *Emissivity Table*. July 2015. URL: `https://www.calex.co.uk/site/wp-content/uploads/2015/07/emissivity-tables.pdf`.

[55] L. L. C. Engineers Edge. *Thermal Properties of Metals, Conductivity, Thermal Expansion, Specific Heat*. Ed. by L. L. C. Engineers Edge. 2021. URL: `https://www.engineersedge.com/properties_of_metals.htm`.

[56] Xiaocui Zhang et al. "Effects of Computational Domain on Numerical Simulation of Building Fires". In: *Journal of Fire Protection Engineering* 20.4 (2010), pp. 225–251. DOI: `10.1177/1042391510367349`.

[57] K. D. Steckler, J. G. Quintiere, and W. J. Rinkinen. "Flow induced by fire in a compartment". In: *Symposium (International) on Combustion* 19.1 (1982). Nineteenth Symposium (International) on Combustion, pp. 913–920. ISSN: 0082-0784. DOI: `https://doi.org/10.1016/S0082-0784(82)80267-1`.

[58] Bjarne Hustedt, T. Hertzberg, and G. Holmstedt. "The physics behind water mist systems". In: 2004.

[59] Kevin McGrattan et al. "Fire dynamics simulator, user's guide". In: *NIST special publication 1019* 1019.6 (Aug. 21, 2020). eprint: `https://github.com/firemodels/fds/releases/download/FDS6.7.5/FDS_User_Guide.pdf`.

Appendices

Appendix A

An FDS Input for Solid Phase Simulations

```
&HEAD CHID='DM_10', TITLE='Cu plate only' / cell size=1cm

&MESH ID='mesh1', IJK=30,30,30, XB=-0.15,0.15,-0.15,0.15,-0.05,0.25 /

&TIME T_END=2000.0 /

&MISC TMPA=20.0 /

&OBST XB= -0.1,0.1,-0.1,0.1,0.0,0.0, SURF_ID='Cu plate',
    COLOR='BLACK', THICKEN=.TRUE.  /

&MATL ID='Cu'
        CONDUCTIVITY=401
        SPECIFIC_HEAT=0.385
        DENSITY=8960 /

&SURF ID='Cu plate'
        MATL_ID='Cu'
        THICKNESS=0.005
        EMISSIVITY=0.78
        BACKING='INSULATED'
        CONVECTION_LENGTH_SCALE=0.2
        EXTERNAL_FLUX=37.3 /

&VENT DB='XMIN', SURF_ID='OPEN' /
&VENT DB='XMAX', SURF_ID='OPEN' /
&VENT DB='YMIN', SURF_ID='OPEN' /
&VENT DB='YMAX', SURF_ID='OPEN' /
&VENT DB='ZMIN', SURF_ID='OPEN' /
&VENT DB='ZMAX', SURF_ID='OPEN' /

&DEVC ID='Tp 00', XYZ=0.00,0.0,0.0, IOR=-3, QUANTITY='WALL
    TEMPERATURE' /
&DEVC ID='Tp 20', XYZ=0.02,0.0,0.0, IOR=-3, QUANTITY='WALL
    TEMPERATURE' /
```

```
&DEVC ID='Tp 40', XYZ=0.04,0.0,0.0, IOR=-3, QUANTITY='WALL
    TEMPERATURE' /
&DEVC ID='Tp 60', XYZ=0.06,0.0,0.0, IOR=-3, QUANTITY='WALL
    TEMPERATURE' /
&DEVC ID='Tp 80', XYZ=0.08,0.0,0.0, IOR=-3, QUANTITY='WALL
    TEMPERATURE' /

&SLCF PBY=0, QUANTITY='TEMPERATURE' /
&SLCF PBY=0, QUANTITY='W-VELOCITY' /

&DUMP DT_DEVC=10.0 /

&TAIL /
```

Appendix B

An FDS Input for Water Phase Simulations

```
&HEAD CHID='size2_spr', TITLE='water mist system only' / cell
   size=1cm

&MESH ID='mesh1', IJK=30,30,7, XB=-0.15,0.15,-0.15,0.15,-0.05,0.02,
   MPI_PROCESS=0 /
&MESH ID='mesh2', IJK=30,30,7, XB=-0.15,0.15,-0.15,0.15,0.02,0.09,
   MPI_PROCESS=1 /
&MESH ID='mesh3', IJK=30,30,7, XB=-0.15,0.15,-0.15,0.15,0.09,0.16,
   MPI_PROCESS=2 /
&MESH ID='mesh4', IJK=30,30,7, XB=-0.15,0.15,-0.15,0.15,0.16,0.23,
   MPI_PROCESS=3 /
&MESH ID='mesh5', IJK=30,30,7, XB=-0.15,0.15,-0.15,0.15,0.23,0.30,
   MPI_PROCESS=4 /

&TIME T_END=110.0 /

&MISC TMPA=20.0 /

&VENT DB='XMIN', SURF_ID='OPEN' /
&VENT DB='XMAX', SURF_ID='OPEN' /
&VENT DB='YMIN', SURF_ID='OPEN' /
&VENT DB='YMAX', SURF_ID='OPEN' /
&VENT DB='ZMIN', SURF_ID='OPEN' /
&VENT DB='ZMAX', SURF_ID='OPEN' /

&SPEC ID='WATER VAPOR' /

&PART ID='watermist', SPEC_ID='WATER VAPOR', DIAMETER=140,
   MONODISPERSE=.TRUE. /

&PROP ID='sprinkler',
         PART_ID='watermist',
         OFFSET=0.01,
         SPRAY_ANGLE=0,65,
         FLOW_RATE=0.0231,
```

```
            PARTICLE_VELOCITY=20,
            FLOW_RAMP='SPRAMP',
            PARTICLES_PER_SECOND=5000.0 /

&RAMP ID='SPRAMP', T=0.0, F=0.0 /
&RAMP ID='SPRAMP', T=1.0, F=1.0 /


&DEVC ID='SPR', XYZ=0.0,0.0,0.25, PROP_ID='sprinkler',
   QUANTITY='TIME', SETPOINT=0.0 /


&PROP ID='pdpa_SMD',
      PART_ID     = 'watermist',
      QUANTITY    = 'DIAMETER',
      PDPA_RADIUS = 0.01,
      PDPA_START  = 10.0,
      PDPA_END    = 110.0,
      PDPA_M      = 3,
      PDPA_N      = 2 /


&DEVC XYZ= 0.00,0.0,0.01, QUANTITY='PDPA', PROP_ID='pdpa_SMD',
   ID='SMD1-0' /
&DEVC XYZ= 0.01,0.0,0.01, QUANTITY='PDPA', PROP_ID='pdpa_SMD',
   ID='SMD1-10' /
&DEVC XYZ= 0.02,0.0,0.01, QUANTITY='PDPA', PROP_ID='pdpa_SMD',
   ID='SMD1-20' /
&DEVC XYZ= 0.03,0.0,0.01, QUANTITY='PDPA', PROP_ID='pdpa_SMD',
   ID='SMD1-30' /
&DEVC XYZ= 0.04,0.0,0.01, QUANTITY='PDPA', PROP_ID='pdpa_SMD',
   ID='SMD1-40' /
&DEVC XYZ= 0.05,0.0,0.01, QUANTITY='PDPA', PROP_ID='pdpa_SMD',
   ID='SMD1-50' /
&DEVC XYZ= 0.06,0.0,0.01, QUANTITY='PDPA', PROP_ID='pdpa_SMD',
   ID='SMD1-60' /
&DEVC XYZ= 0.08,0.0,0.01, QUANTITY='PDPA', PROP_ID='pdpa_SMD',
   ID='SMD1-80' /
&DEVC XYZ= 0.10,0.0,0.01, QUANTITY='PDPA', PROP_ID='pdpa_SMD',
   ID='SMD1-100' /


&PROP ID='pdpa_w',
      PART_ID     = 'watermist',
      QUANTITY    = 'W-VELOCITY',
      PDPA_RADIUS = 0.01,
      PDPA_START  = 10.0,
      PDPA_END    = 110.0,
      PDPA_M      = 0,
      PDPA_N      = 0 /


&DEVC XYZ= 0.00,0.0,0.01, QUANTITY='PDPA', PROP_ID='pdpa_w',
   ID='w1-0' /
&DEVC XYZ= 0.01,0.0,0.01, QUANTITY='PDPA', PROP_ID='pdpa_w',
   ID='w1-10' /
```

```
&DEVC XYZ= 0.02,0.0,0.01, QUANTITY='PDPA', PROP_ID='pdpa_w',
    ID='w1-20' /
&DEVC XYZ= 0.03,0.0,0.01, QUANTITY='PDPA', PROP_ID='pdpa_w',
    ID='w1-30' /
&DEVC XYZ= 0.04,0.0,0.01, QUANTITY='PDPA', PROP_ID='pdpa_w',
    ID='w1-40' /
&DEVC XYZ= 0.05,0.0,0.01, QUANTITY='PDPA', PROP_ID='pdpa_w',
    ID='w1-50' /
&DEVC XYZ= 0.06,0.0,0.01, QUANTITY='PDPA', PROP_ID='pdpa_w',
    ID='w1-60' /
&DEVC XYZ= 0.08,0.0,0.01, QUANTITY='PDPA', PROP_ID='pdpa_w',
    ID='w1-80' /
&DEVC XYZ= 0.1,0.0,0.01, QUANTITY='PDPA', PROP_ID='pdpa_w',
    ID='w1-100' /

&DUMP DT_DEVC=10.0 /

&TAIL /
```

Appendix C

An FDS Input for Solid and Water phases Combined Simulations

```
&HEAD CHID='size2', TITLE='Cu plate and water droplets' / cell
   size=1cm

&MESH ID='mesh1', IJK=30,30,7, XB=-0.15,0.15,-0.15,0.15,-0.05,0.02,
   MPI_PROCESS=0 /
&MESH ID='mesh2', IJK=30,30,7, XB=-0.15,0.15,-0.15,0.15,0.02,0.09,
   MPI_PROCESS=1 /
&MESH ID='mesh3', IJK=30,30,7, XB=-0.15,0.15,-0.15,0.15,0.09,0.16,
   MPI_PROCESS=2 /
&MESH ID='mesh4', IJK=30,30,7, XB=-0.15,0.15,-0.15,0.15,0.16,0.23,
   MPI_PROCESS=3 /
&MESH ID='mesh5', IJK=30,30,7, XB=-0.15,0.15,-0.15,0.15,0.23,0.30,
   MPI_PROCESS=4 /

&TIME T_END=4500.0 /

&MISC TMPA=20.0 /

&OBST XB= -0.1,0.1,-0.1,0.1,0.0,0.0, SURF_ID='Cu plate',
   COLOR='BLACK', THICKEN=.TRUE.  /

&MATL ID='Cu'
        CONDUCTIVITY=401
        SPECIFIC_HEAT=0.385
        DENSITY=8960 /

&SURF ID='Cu plate'
        MATL_ID='Cu'
        THICKNESS=0.005
        EMISSIVITY=0.78
        BACKING='INSULATED'
        CONVECTION_LENGTH_SCALE=0.2
        EXTERNAL_FLUX=38.3 /

&VENT DB='XMIN', SURF_ID='OPEN' /
```

```
&VENT DB='XMAX', SURF_ID='OPEN' /
&VENT DB='YMIN', SURF_ID='OPEN' /
&VENT DB='YMAX', SURF_ID='OPEN' /
&VENT DB='ZMIN', SURF_ID='OPEN' /
&VENT DB='ZMAX', SURF_ID='OPEN' /


&SPEC ID='WATER VAPOR' /

&PART ID='watermist', SPEC_ID='WATER VAPOR', DIAMETER=140,
   MONODISPERSE=.TRUE., HEAT_TRANSFER_COEFFICIENT_SOLID=-1 /

&PROP ID='sprinkler',
         PART_ID='watermist',
         OFFSET=0.01,
         SPRAY_ANGLE=0,65,
         FLOW_RATE=0.0231,
         PARTICLE_VELOCITY=20,
         FLOW_RAMP='SPRAMP',
         PARTICLES_PER_SECOND=5000.0 /

&RAMP ID='SPRAMP', T=0.0, F=0.0 /
&RAMP ID='SPRAMP', T=1999.0, F=0.0 /
&RAMP ID='SPRAMP', T=2000.0, F=1.0 /

&DEVC ID='SPR', XYZ=0.0,0.0,0.25, PROP_ID='sprinkler',
   QUANTITY='TIME', SETPOINT=0.0 /

&PROP ID='pdpa_SMDi',
      PART_ID        = 'watermist',
      QUANTITY       = 'DIAMETER',
      PDPA_RADIUS    = 0.01,
      PDPA_START     = 2000.0,
      PDPA_END       = 4500.0,
      PDPA_M         = 1,
      PDPA_INTEGRATE = .FALSE. /

&DEVC XYZ= 0.00,0.0,0.01, QUANTITY='PDPA', PROP_ID='pdpa_SMDi',
   ID='iD1 0' /
&DEVC XYZ= 0.01,0.0,0.01, QUANTITY='PDPA', PROP_ID='pdpa_SMDi',
   ID='iD1 10' /
&DEVC XYZ= 0.02,0.0,0.01, QUANTITY='PDPA', PROP_ID='pdpa_SMDi',
   ID='iD1 20' /
&DEVC XYZ= 0.03,0.0,0.01, QUANTITY='PDPA', PROP_ID='pdpa_SMDi',
   ID='iD1 30' /
&DEVC XYZ= 0.04,0.0,0.01, QUANTITY='PDPA', PROP_ID='pdpa_SMDi',
   ID='iD1 40' /
&DEVC XYZ= 0.05,0.0,0.01, QUANTITY='PDPA', PROP_ID='pdpa_SMDi',
   ID='iD1 50' /
&DEVC XYZ= 0.06,0.0,0.01, QUANTITY='PDPA', PROP_ID='pdpa_SMDi',
   ID='iD1 60' /
&DEVC XYZ= 0.08,0.0,0.01, QUANTITY='PDPA', PROP_ID='pdpa_SMDi',
```

```
      ID='iD1 80' /
&DEVC XYZ= 0.10,0.0,0.01, QUANTITY='PDPA', PROP_ID='pdpa_SMDi',
      ID='iD1 100' /


&DEVC XYZ= -0.01,0.0,0.01, QUANTITY='PDPA', PROP_ID='pdpa_SMDi',
      ID='iD1 -10' /
&DEVC XYZ= -0.02,0.0,0.01, QUANTITY='PDPA', PROP_ID='pdpa_SMDi',
      ID='iD1 -20' /
&DEVC XYZ= -0.03,0.0,0.01, QUANTITY='PDPA', PROP_ID='pdpa_SMDi',
      ID='iD1 -30' /
&DEVC XYZ= -0.04,0.0,0.01, QUANTITY='PDPA', PROP_ID='pdpa_SMDi',
      ID='iD1 -40' /
&DEVC XYZ= -0.05,0.0,0.01, QUANTITY='PDPA', PROP_ID='pdpa_SMDi',
      ID='iD1 -50' /
&DEVC XYZ= -0.06,0.0,0.01, QUANTITY='PDPA', PROP_ID='pdpa_SMDi',
      ID='iD1 -60' /
&DEVC XYZ= -0.08,0.0,0.01, QUANTITY='PDPA', PROP_ID='pdpa_SMDi',
      ID='iD1 -80' /
&DEVC XYZ= -0.10,0.0,0.01, QUANTITY='PDPA', PROP_ID='pdpa_SMDi',
      ID='iD1 - 100' /


&PROP ID='pdpa_w',
      PART_ID        = 'watermist',
      QUANTITY       = 'W-VELOCITY',
      PDPA_RADIUS    = 0.01,
      PDPA_START     = 2000.0,
      PDPA_END       = 4500.0,
      PDPA_M         =3,
      PDPA_N         =2,
      PDPA_INTEGRATE = .FALSE. /

&DEVC XYZ= 0.00,0.0,0.01, QUANTITY='PDPA', PROP_ID='pdpa_w', ID='w1
   00' /
&DEVC XYZ= 0.01,0.0,0.01, QUANTITY='PDPA', PROP_ID='pdpa_w', ID='w1
   10' /
&DEVC XYZ= 0.02,0.0,0.01, QUANTITY='PDPA', PROP_ID='pdpa_w', ID='w1
   20' /
&DEVC XYZ= 0.03,0.0,0.01, QUANTITY='PDPA', PROP_ID='pdpa_w', ID='w1
   30' /
&DEVC XYZ= 0.04,0.0,0.01, QUANTITY='PDPA', PROP_ID='pdpa_w', ID='w1
   40' /
&DEVC XYZ= 0.05,0.0,0.01, QUANTITY='PDPA', PROP_ID='pdpa_w', ID='w1
   50' /
&DEVC XYZ= 0.06,0.0,0.01, QUANTITY='PDPA', PROP_ID='pdpa_w', ID='w1
   60' /
&DEVC XYZ= 0.08,0.0,0.01, QUANTITY='PDPA', PROP_ID='pdpa_w', ID='w1
   80' /
&DEVC XYZ= 0.10,0.0,0.01, QUANTITY='PDPA', PROP_ID='pdpa_w', ID='w1
   100' /


==================temperature of the water droplets
```

```
&PROP ID='pdpa_T',
        PART_ID='watermist',
        QUANTITY='TEMPERATURE',
        PDPA_RADIUS=0.005,
        PDPA_START=2000.0,
        PDPA_M=0,
        PDPA_N=0,
        PDPA_END=4500.0 /

&DEVC XYZ=0.00,0.0,0.01, QUANTITY='PDPA', PROP_ID='pdpa_T', ID='T
    00' /
&DEVC XYZ=0.01,0.0,0.01, QUANTITY='PDPA', PROP_ID='pdpa_T', ID='T
    10' /
&DEVC XYZ=0.02,0.0,0.01, QUANTITY='PDPA', PROP_ID='pdpa_T', ID='T
    20' /
&DEVC XYZ=0.03,0.0,0.01, QUANTITY='PDPA', PROP_ID='pdpa_T', ID='T
    30' /
&DEVC XYZ=0.04,0.0,0.01, QUANTITY='PDPA', PROP_ID='pdpa_T', ID='T
    40' /
&DEVC XYZ=0.05,0.0,0.01, QUANTITY='PDPA', PROP_ID='pdpa_T', ID='T
    50' /
&DEVC XYZ=0.06,0.0,0.01, QUANTITY='PDPA', PROP_ID='pdpa_T', ID='T
    60' /
&DEVC XYZ=0.07,0.0,0.01, QUANTITY='PDPA', PROP_ID='pdpa_T', ID='T
    70' /
&DEVC XYZ=0.08,0.0,0.01, QUANTITY='PDPA', PROP_ID='pdpa_T', ID='T
    80' /
&DEVC XYZ=0.09,0.0,0.01, QUANTITY='PDPA', PROP_ID='pdpa_T', ID='T
    90' /
&DEVC XYZ=0.10,0.0,0.01, QUANTITY='PDPA', PROP_ID='pdpa_T', ID='T
    100' /

&DEVC XYZ=-0.01,0.0,0.01, QUANTITY='PDPA', PROP_ID='pdpa_T', ID='T
    -10' /
&DEVC XYZ=-0.02,0.0,0.01, QUANTITY='PDPA', PROP_ID='pdpa_T', ID='T
    -20' /
&DEVC XYZ=-0.03,0.0,0.01, QUANTITY='PDPA', PROP_ID='pdpa_T', ID='T
    -30' /
&DEVC XYZ=-0.04,0.0,0.01, QUANTITY='PDPA', PROP_ID='pdpa_T', ID='T
    -40' /
&DEVC XYZ=-0.05,0.0,0.01, QUANTITY='PDPA', PROP_ID='pdpa_T', ID='T
    -50' /
&DEVC XYZ=-0.06,0.0,0.01, QUANTITY='PDPA', PROP_ID='pdpa_T', ID='T
    -60' /
&DEVC XYZ=-0.07,0.0,0.01, QUANTITY='PDPA', PROP_ID='pdpa_T', ID='T
    -70' /
&DEVC XYZ=-0.08,0.0,0.01, QUANTITY='PDPA', PROP_ID='pdpa_T', ID='T
    -80' /
&DEVC XYZ=-0.09,0.0,0.01, QUANTITY='PDPA', PROP_ID='pdpa_T', ID='T
    -90' /
```

```
&DEVC XYZ=-0.10,0.0,0.01, QUANTITY='PDPA', PROP_ID='pdpa_T', ID='T
    -100' /

==================number concentrations of water droplets

&PROP ID            ='pdpa_Ni',
      PART_ID       ='watermist',
      QUANTITY      ='NUMBER CONCENTRATION',
      PDPA_RADIUS   =0.005,
      PDPA_START    =2000.0,
      PDPA_END      =4500.0,
      PDPA_INTEGRATE = .FALSE. /

&DEVC XYZ=0.00,0.0,0.01, QUANTITY='PDPA', PROP_ID='pdpa_Ni', ID='iN
    00' /
&DEVC XYZ=0.01,0.0,0.01, QUANTITY='PDPA', PROP_ID='pdpa_Ni', ID='iN
    10' /
&DEVC XYZ=0.02,0.0,0.01, QUANTITY='PDPA', PROP_ID='pdpa_Ni', ID='iN
    20' /
&DEVC XYZ=0.03,0.0,0.01, QUANTITY='PDPA', PROP_ID='pdpa_Ni', ID='iN
    30' /
&DEVC XYZ=0.04,0.0,0.01, QUANTITY='PDPA', PROP_ID='pdpa_Ni', ID='iN
    40' /
&DEVC XYZ=0.05,0.0,0.01, QUANTITY='PDPA', PROP_ID='pdpa_Ni', ID='iN
    50' /
&DEVC XYZ=0.06,0.0,0.01, QUANTITY='PDPA', PROP_ID='pdpa_Ni', ID='iN
    60' /
&DEVC XYZ=0.07,0.0,0.01, QUANTITY='PDPA', PROP_ID='pdpa_Ni', ID='iN
    70' /
&DEVC XYZ=0.08,0.0,0.01, QUANTITY='PDPA', PROP_ID='pdpa_Ni', ID='iN
    80' /
&DEVC XYZ=0.09,0.0,0.01, QUANTITY='PDPA', PROP_ID='pdpa_Ni', ID='iN
    90' /
&DEVC XYZ=0.10,0.0,0.01, QUANTITY='PDPA', PROP_ID='pdpa_Ni', ID='iN
    100' /

&DEVC XYZ=-0.01,0.0,0.01, QUANTITY='PDPA', PROP_ID='pdpa_Ni', ID='iN
    -10' /
&DEVC XYZ=-0.02,0.0,0.01, QUANTITY='PDPA', PROP_ID='pdpa_Ni', ID='iN
    -20' /
&DEVC XYZ=-0.03,0.0,0.01, QUANTITY='PDPA', PROP_ID='pdpa_Ni', ID='iN
    -30' /
&DEVC XYZ=-0.04,0.0,0.01, QUANTITY='PDPA', PROP_ID='pdpa_Ni', ID='iN
    -40' /
&DEVC XYZ=-0.05,0.0,0.01, QUANTITY='PDPA', PROP_ID='pdpa_Ni', ID='iN
    -50' /
&DEVC XYZ=-0.06,0.0,0.01, QUANTITY='PDPA', PROP_ID='pdpa_Ni', ID='iN
    -60' /
&DEVC XYZ=-0.07,0.0,0.01, QUANTITY='PDPA', PROP_ID='pdpa_Ni', ID='iN
    -70' /
&DEVC XYZ=-0.08,0.0,0.01, QUANTITY='PDPA', PROP_ID='pdpa_Ni', ID='iN
```

```
    -80' /
&DEVC XYZ=-0.09,0.0,0.01, QUANTITY='PDPA', PROP_ID='pdpa_Ni', ID='iN
    -90' /
&DEVC XYZ=-0.10,0.0,0.01, QUANTITY='PDPA', PROP_ID='pdpa_Ni', ID='iN
    -100' /


==================slice files

&SLCF PBY=0, QUANTITY='TEMPERATURE' /
&SLCF PBY=0, QUANTITY='W-VELOCITY' /


=================boundary files

&BNDF QUANTITY='WALL TEMPERATURE' /
&BNDF QUANTITY='NET HEAT FLUX' /
&BNDF QUANTITY='RADIATIVE HEAT FLUX' /
&BNDF QUANTITY='CONVECTIVE HEAT FLUX' /


==================temperature of the Cu plate

&DEVC ID='Tp 00', XYZ=0.00,0.0,0.0, QUANTITY='WALL TEMPERATURE',
    IOR=3 /
&DEVC ID='Tp 10', XYZ=0.01,0.0,0.0, QUANTITY='WALL TEMPERATURE',
    IOR=3 /
&DEVC ID='Tp 20', XYZ=0.02,0.0,0.0, QUANTITY='WALL TEMPERATURE',
    IOR=3 /
&DEVC ID='Tp 30', XYZ=0.03,0.0,0.0, QUANTITY='WALL TEMPERATURE',
    IOR=3 /
&DEVC ID='Tp 40', XYZ=0.04,0.0,0.0, QUANTITY='WALL TEMPERATURE',
    IOR=3 /
&DEVC ID='Tp 50', XYZ=0.05,0.0,0.0, QUANTITY='WALL TEMPERATURE',
    IOR=3 /
&DEVC ID='Tp 60', XYZ=0.06,0.0,0.0, QUANTITY='WALL TEMPERATURE',
    IOR=3 /
&DEVC ID='Tp 70', XYZ=0.07,0.0,0.0, QUANTITY='WALL TEMPERATURE',
    IOR=3 /
&DEVC ID='Tp 80', XYZ=0.08,0.0,0.0, QUANTITY='WALL TEMPERATURE',
    IOR=3 /
&DEVC ID='Tp 90', XYZ=0.09,0.0,0.0, QUANTITY='WALL TEMPERATURE',
    IOR=3 /

&DEVC ID='Tp -10', XYZ=-0.01,0.0,0.0, QUANTITY='WALL TEMPERATURE',
    IOR=3 /
&DEVC ID='Tp -20', XYZ=-0.02,0.0,0.0, QUANTITY='WALL TEMPERATURE',
    IOR=3 /
&DEVC ID='Tp -30', XYZ=-0.03,0.0,0.0, QUANTITY='WALL TEMPERATURE',
    IOR=3 /
&DEVC ID='Tp -40', XYZ=-0.04,0.0,0.0, QUANTITY='WALL TEMPERATURE',
    IOR=3 /
&DEVC ID='Tp -50', XYZ=-0.05,0.0,0.0, QUANTITY='WALL TEMPERATURE',
    IOR=3 /
```

```
&DEVC ID='Tp -60', XYZ=-0.06,0.0,0.0, QUANTITY='WALL TEMPERATURE',
    IOR=3 /
&DEVC ID='Tp -70', XYZ=-0.07,0.0,0.0, QUANTITY='WALL TEMPERATURE',
    IOR=3 /
&DEVC ID='Tp -80', XYZ=-0.08,0.0,0.0, QUANTITY='WALL TEMPERATURE',
    IOR=3 /
&DEVC ID='Tp -90', XYZ=-0.09,0.0,0.0, QUANTITY='WALL TEMPERATURE',
    IOR=3 /

&DUMP DT_DEVC=10.0, DT_SLCF=10.0, DT_BNDF=10.0 /

&TAIL /
```